HHS Public Access

Author manuscript

*J Magn Reson Imaging*. Author manuscript; available in PMC 2016 September 01.

Published in final edited form as:

*J Magn Reson Imaging*. 2015 September ; 42(3): 545–565. doi:10.1002/jmri.24787.

# "Basic MR Relaxation Mechanisms & Contrast Agent Design"

**Luis M. De León-Rodríguez, PhD**[1], **André F. Martins, PhD**[2], **Marco Pinho, MD**[3], **Neil Rofsky, MD**[3], and **A. Dean Sherry, PhD**[2,3]

[1]The University of Auckland, 23 Symonds St., Auckland 1142, New Zealand [2]Department of Chemistry, University of Texas at Dallas, 2601 N. Floyd Road, Richardson, TX 75080, USA [3]Department of Radiology and the Advanced Imaging Research Center, University of Texas Southwestern Medical Center, 5323 Harry Hines Blvd, NE 4.2, Dallas, TX 75390-8568, USA

## Abstract

The diagnostic capabilities of magnetic resonance imaging (MRI) have undergone continuous and substantial evolution by virtue of hardware and software innovations and the development and implementation of exogenous contrast media. Thirty years since the first MRI contrast agent was approved for clinical use, a reliance on MR contrast media persists largely to improve image quality with higher contrast resolution and to provide additional functional characterization of normal and abnormal tissues. Further development of MR contrast media is an important component in the quest for continued augmentation of diagnostic capabilities. In this review we will detail the many important considerations when pursuing the design and use of MR contrast media. We will offer a perspective on the importance of chemical stability, particularly kinetic stability, and how this influences one's thinking about the safety of metal-ligand based contrast agents. We will discuss the mechanisms involved in magnetic resonance relaxation in the context of probe design strategies. A brief description of currently available contrast agents will be accompanied by an in-depth discussion that highlights promising MRI contrast agents in development for future clinical and research applications. Our intention is to give a diverse audience an improved understanding of the factors involved in developing new types of safe and highly efficient MR contrast agents and, at the same time, provide an appreciation of the insights into physiology and disease that newer types of responsive agents can provide.

### Keywords

gadolinium MRI contrast agents; thermodynamic and kinetic principles; $T_1$ and $T_2$ contrast agents; CEST agents; responsive contrast agents; smart contrast agents; targeted contrast agents; clinical MRI contrast agents; in vivo MRI

## 1. INTRODUCTION

Image contrast in magnetic resonance (MR), the difference in signal intensity between tissues or anatomic spaces, can be enhanced or augmented by manipulation of imaging

sherry@utdallas.edu; Fax: + 01 972-883-2925; Tel: + 01 972-883-29072. dean.sherry@utsouthwestern.edu; Fax: + 01 214-645-2744; Tel: + 01 214-645-2720.

parameters and/ or by the introduction of certain chemical (contrast) agents that influence the relaxation of water, the most abundant substance in human tissues. Such agents have proliferated because of their ability to facilitate detection and characterization of normal *versus* diseased tissues. Continued development of contrast agents (CA) is an important component of our efforts to increase the value proposition of MR technology. Such development entails considering a complex set of parameters, many of which interact with one another often involving trade-offs among those parameters. The objective of this review is to summarize insights into lanthanide ion chemistry that will offer an appreciation for the challenges faced when trying to generate clinically safe, effective and highly sensitive agents. Furthermore, it is intended that the reader also gains insight into the challenges and opportunities surrounding newer types of responsive MR agents that can provide additional physiological and biochemical information for diagnostic imaging. Given the diverse audience which will include readers that may not have a detailed chemistry background or familiarity with the relevant nomenclature, certain words have been underlined to indicate their presence in a glossary section that describes the words and related concepts.

## 2. Current MRI Contrast Agents

MRI contrast agents (CA) have been widely used in diagnostic imaging for nearly 30 years. Most current CA are either simple paramagnetic metal ion-ligand (ML) complexes or superparamagnetic particles, both of which alter image contrast by decreasing the $T_1$ and $T_2$ of water protons. The first paramagnetic complex approved in 1987 for use in cancer patients to detect brain tumors was gadolinium(III) diethylenetetraamine pentaacetic acid (GdDTPA). This first approval stimulated intense world-wide interest into understanding the precise physical-chemical mechanisms by which these agents work *in vivo*. This in turn led to new chemical insights into how to maximize the sensitivity of such agents and, more importantly, how to create responsive or smart agents that can potentially provide added biochemical or physiological information to aid in a clinical diagnosis.

### 2.1. $T_1$-based Contrast Agents

$T_1$-based contrast agents are exogenous paramagnetic metal ion complexes that shorten the longitudinal relaxation time of surrounding water protons. These are also referred to as "positive" agents because they typically produce image brightening in $T_1$-weighted imaging sequences. The gadolinium ion ($Gd^{3+}$) which lies in the middle of the lanthanide (Ln) family of elements is the metal of choice for nearly all $T_1$-based agents because it has 7 unpaired electrons in its 4f orbitals, a high magnetic moment ($\mu^2 = 63\ BM^2$) and a unusually long electronic spin relaxation time (1,2). This makes relaxation of any nearby water protons efficient on a per mole basis. The "free" or unchelated $Gd^{3+}$ ion is toxic in most biological systems largely because the ion has ionic radius close to that of $Ca^{2+}$ but also a higher positive charge. Consequently, proteins cannot distinguish between a $Gd^{3+}$ *versus* $Ca^{2+}$ ion so any free $Gd^{3+}$ introduced into a biological system quickly binds to $Ca^{2+}$ ion channels and other $Ca^{2+}$ requiring proteins such as calmodulin, calsequistrin, and calexitin. The mechanisms involved for $Gd^{3+}$ toxicity are however still not very well understood (3–6). To suppress potential toxicity, $Gd^{3+}$ must be held tightly by an organic ligand to form a ML complex or chelate. The ligand influences the chemistry of $Gd^{3+}$ by 1) reducing toxicity, 2)

altering the tissue distribution of the agent, and 3) influencing the efficiency of $Gd^{3+}$ in shortening $T_1$ and $T_2$.

From a safety perspective, the resulting ML complexes must be thermodynamically stable (Table 1) and, more importantly for *in vivo* use, kinetically inert. The thermodynamic stability of a $Gd^{3+}$ complex, defined by the equilibrium constant, $K_{st}$, is a measure of how much free, uncomplexed $Gd^{3+}$ ion will be released in a biological environment if the system reaches "equilibrium". The word "equilibrium" is emphasized here because these ML complexes often are not in the body long enough to reach any new thermodynamic equilibrium that might take place as a result of the ML complex experiencing some new biological environment, such as a region of low tissue pH for example. If kidney filtration is adequate, even complexes with log $K_{st}$ values well below those shown in Table 1 are excreted long before any small amount of free $Gd^{3+}$ can be released. This is why understanding the kinetics of complex dissociation is so important. The kinetic stability of any complex refers to how fast or slow a $Gd^{3+}$ ion is released from a ML complex as reflected by the rate constant, $k_{obs}$ or $k_1$ (Table 1).

To facilitate understanding of thermodynamic versus kinetic stability, we can consider an analogy with conversion of diamond to graphite. While this conversion is thermodynamically favorable because the free energy of graphite is lower than that of diamond, it doesn't readily occur under ordinary conditions because the kinetics of the reaction (requiring immense activation energy) is extremely slow. Thus, thermodynamic stability determines whether a given reaction is favorable (i.e., spontaneous), but says nothing about the likelihood that the reaction will take place over a given period of time. If a reaction takes place extremely slowly compared to the amount of time a ML complex remains in the body for example, then the reaction is considered kinetically inert. Unfortunately, the importance of kinetic inertness was not fully appreciated in the original design of MR contrast agents, so it wasn't until the emergence of nephrogenic systemic fibrosis (NSF) that the importance of kinetic stability was fully appreciated. It is now known that macrocyclic ligands have substantial advantages over linear polyamino-based ligands simply because the former are much more kinetically inert toward dissociation (3,5,28,29). Other factors such as transmetallation processes can occur in the presence of endogenous metal ions ($Zn^{2+}$, $Ca^{2+}$, $Cu^{2+}$, etc.) and other endogenous ligands (lactate, bicarbonate, phosphate, etc.) can also influence the kinetics of complex dissociation but, here again, it has been demonstrated that macrocyclic-based ML complexes have an advantage as well (30).

Most FDA approved and commercially available $T_1$ contrast agents at the time of this writing are gadolinium-based complexes derived from various polyaminocarboxylate ligands. Macrocyclic polyaminocarboxylate ligands like DOTA and HP-DO3A have been shown to form $Gd^{3+}$ complexes with high thermodynamic stability and kinetic inertness (Figure 1) (31). Some linear ligands like DTPA also form very stable complexes with $Gd^{3+}$, with thermodynamic stability constants quite similar to some macrocyclic complexes (compare GdDTPA with GdDO3A-butrol, for example, Table 1). However, the bis-amide derivatives of DTPA form much less stable complexes with $Gd^{3+}$ (see log $K_{st}$ values for GdDTPA-BMA and GdDTPA-BMEA, Table 1) and these agents, were the ones most

frequently used in NSF patients. Thus, although thermodynamics was considered the most important factor initially, the agents most often used in NSF patients solidified the now accepted fact that the kinetic inertness of a complex is likely *more important* than its thermodynamic stability. This was originally suggested by Tweedle, *et al.* (11) very early during contrast agent development and remains an extremely important concept to consider when developing newer types of contrast agents (responsive agents, targeted agents, MR-PET agents). This is further supported by the results of Wedeking *et al.* who reported an inverse proportionality between $k_{obs}$ and the total residual $Gd^{3+}$ found in the bodies of mice (11).

The efficiency of a $T_1$ MR contrast agent is defined by its relaxivity, $r_1$, the longitudinal paramagnetic relaxation rate ($R_1 = 1/T_1$) observed for a 1 mM aqueous solution of contrast media. $r_1$ is reported in units of $mM^{-1}s^{-1}$ and is field and temperature dependent.

$$\frac{1}{T_{1obs}} = \frac{1}{T_{1d}} + \frac{1}{T_{1p}} \quad [1]$$

$$\frac{1}{T_{1obs}} = \frac{1}{T_{1d}} + r_1[Gd \quad [2]$$

$$r_1 = r_1^{IS} + r_1^{OS} \quad [3]$$

Here $1/T_{1obs}$ represents the observed water proton relaxation rate, $1/T_{1d}$ is the diamagnetic water proton relaxation rate and $1/T_{1p}$ is the paramagnetic contribution. $1/T_{1d}$ is measured in the same conditions as $1/T_{1obs}$ but in the absence of the paramagnetic complex (solvent contribution). The relaxivity is composed of an inner sphere (IS) and an outer sphere (OS) term (Equation [3]). The inner sphere term describes the relaxation effect originating from the closest hydrogen nuclei of water molecules interacting directly with the paramagnetic ion, while the outer sphere term describes the effect of the interactions between the paramagnetic ion and closely diffusing water molecules without interacting with the complex (the outer sphere). In some cases, water molecules weakly interacting with the ligand might constitute a second hydration sphere, which can lead to a second sphere relaxivity term, see Figure 2). For clinical agents, approximately 60% of the relaxivity originates from inner sphere relaxation and 40% from outer sphere effects.

The inner sphere relaxivity term is linearly proportional to the hydration number (q) of the $Gd^{3+}$ complex. The agent structures shown in Figure 1 are all monohydrated complexes (q = 1). This means that there is only enough space remaining around the $Gd^{3+}$ for a single water molecule after the ligand occupies most of the possible coordination sites. This single, inner-sphere water molecule is not tightly bound to the $Gd^{3+}$ ion but is dynamic and exchanges, usually rapidly, with other nearby water molecules in the bulk solvent. A few complexes with larger hydration numbers (q = 2 or 3), such as the GdHOPO derivatives and GdAAZTA (32,33), have been studied as MRI contrast agents but, in general, increasing the hydration number often compromises the thermodynamic and/or kinetic stability of the

complexes thereby making them more vulnerable to transmetallation or transchelation with endogenous metal ions or anions. This has been found to be especially true whenever two water molecules are in a *cis* position in the $Gd^{3+}$ coordination sphere (30). In addition to the hydration number, other parameters that govern the efficiency of a given MR contrast agent can be also optimized: the Gd-H distance, $r_{GdH}$; the water exchange rate, $k_{ex} = 1/\tau_m$, where $\tau_m$ is the mean lifetime of the water molecule(s) in the inner sphere of the metal ion; the rotational correlation time, $\tau_R$ (often referred to as 'tumbling'); the electronic spin relaxation times, $T_{1e}$ and $T_{2e}$ (Figure 2).

### 2.2. $T_2$-based Contrast Agents

$T_2$ contrast agents decrease the water signal intensity by shortening the transverse relaxation times. The large anisotropic magnetic susceptibility induced by these agents create local magnetic field gradients which efficiently dephase the transverse magnetization. The efficiency of a $T_2$ MR contrast agent is defined by its relaxivity, $r_2$, the transverse relaxation rate ($r_2 = 1/T_2$) observed for 1 mM solution of contrast media in water. Given the growth of higher magnetic field MRI scanners in clinical practice, $T_2$ contrast mechanisms due to endogenous and exogenous iron (iron oxide particles) have gained increased relevance. While studies have shown that the $r_1$ relaxivities of low molecular weight $T_1$-based contrast agents are typically lower at high magnetic fields ($B_o$), the intrinsic $T_1$ of tissue water is also longer at higher fields so the net efficiency of $T_1$-based CA is not overly compromised, at least at field strengths that could become clinical over the next decade (up to 7T). Conversely, $T_2$ contrast agents can be an efficient solution for high field applications since the transverse relaxivity ($r_2$) increases at higher fields.

Currently, the majority of $T_2$ contrast agents are iron oxide-based superparamagnetic nanoparticles coated with dextran, silicates or other non-immunogenic polymers. Surface coating is useful not only for insuring biocompatibility but also because most of the polymer coatings can be functionalized for selective targeting, multimodality and therapy applications (34–37). In fact, depending on the coating identity and the size of iron-oxide particles, one can identify SPIO (Superparamagnetic, 50–500nm), USPIO (Ultra small superparamagnetic, 4–50nm), MION (monocrystalline) and CLIO (cross-linked) nanoparticles with quite variable $T_2$ relaxivities and tissue biodistribution (38). The very favorable $T_2$ relaxivities of such nanoparticles makes them attractive for detecting specific biological targets by MRI but their large size can impede or alter tissue penetration and delivery so untargeted SPIO's are the only nanoparticles used clinically to date. Outer-sphere theory for $T_2$ relaxivity predicts that the effectiveness of superparamagnetic particles is highly dependent on both the saturation magnetization (*Ms*) value and the effective radius (*r*) (Equation [4]) (39,40).

$$\frac{1}{T_2} = \left(256\pi^2\gamma^2/405\right).\kappa M_s^2 r^2/D(1+\ell/r) \quad [4]$$

where *D* is the diffusivity of water molecules, $\ell$ is the thickness of an impermeable surface coating, and $k = V^*/C$ where $V^*$ is the volume fraction and *C* is the total iron concentration. In a simplistic way, this equation tells us that increasing $M_s$,, reflected also as the ability of particles to easily be magnetized by the magnetic field, or the magnetic core radius will

result in higher $r_2$ relaxivity (41). Recently, many novel platforms, such as carbon nanotubes (iron oxide doped) (42), zeolites ($Dy^{3+}$ doped) (43) and metal-organic frameworks (MOFS) ($Dy^{3+}$ and $Gd^{3+}$ doped) (44,45) have been studied as potential $T_2$ contrast agents and there is growing interest in CEST and $T_2$-exchange agents because small molecule agents, similar to the $Gd^{3+}$ agents already in use clinically, have some advantages over the larger nanoparticles (46).

It is important to note that all contrast agents shorten both $T_1$ and $T_2$. It is the relative contribution to $r_1$ or $r_2$ that influence contrast agent behavior. For iron agents, several factors contribute such as the crystalline symmetry, the size of the core and the nature of the coating used for the core (47,48). For example, a ferumoxides injectable agent (Feridex®) that had been used for liver imaging, has a crystal aggregate structure with a dextran coating and its large size contributes to a large $r_2$ which provides notable signal reduction when concentrated in the liver. On the other hand Ferumoxam (Sinerem®), an iron oxide composed of smaller particles, has relatively less $r_2$ and more $r_1$, characteristics that can facilitate MRA or other $T_1$-weighted MR techniques (49,50).

**3.2.1. Chemical Exchange Saturation Transfer (CEST) Agents—**This newest class of MR contrast agents is based on protons exchanging between one type of molecule and another. For example, if one dissolves a simple biomolecule such as an amino acid in water, the "exchangeable" $-NH_2$ and $-CO_2H$ protons exchange with water protons at some rate (carboxyl protons exchange fast, amino protons exchange more slowly). In tissue, there are obviously many difference types of such exchangeable protons (every biomolecule that contains a –NH, $-NH_2$, or -OH proton) each in exchange with water protons and each at a different rate. This phenomenon provides an opportunity to generate MRI contrast by a unique mechanism as illustrated in Figure 3A. In this example, protons in pool B (assume this represents a specific type of $-NH_2$ group on a protein) are exchanging with protons in pool A (water) at some slow rate (51). The basic requirement for using this phenomenon as a method to produce MR contrast is that the chemical shift between the exchanging $-NH_2$ protons and bulk water ($\Delta\omega$) must be large enough to allow frequency-selective saturation of the $-NH_2$ resonance without also saturation the water protons. If this requirement is met, then selective saturation of the $-NH_2$ protons for a period of time (typically 1–5 s) results in a decrease in intensity of the water signal ($M_z/M_o$) because some of the saturated $-NH_2$ protons enter the pool of water protons during this saturation period (52). The decrease in water intensity after reaching a new equilibrium is given by:

$$\frac{M_z}{M_o} = \frac{100}{1 + \frac{cqT_1}{55.5\tau_m}} \quad [5]$$

From an imaging perspective, the decrease in water intensity produced by CEST has the same net effect as a classical $T_2$ agent, i.e., the water intensity decreases and the image darkens. However, one great advantage of CEST over iron-based $T_2$ contrast agents is that the CEST signal can be turned "on" and "off" by the operator using the frequency-selective presaturation pulse. Consequently, the scientific interest in CEST, especially endogenous CEST contrast, is growing rapidly (46,52,53). Two examples of the use of CEST imaging to detect some specific biological process are illustrated in Figure 3. The first example

illustrates an endogenous CEST signal that arises after selective presaturation of all exchanging –NH protons (53). The resulting change in water intensity (the CEST signal) is significantly higher in tumor that normal brain and, perhaps more importantly from a diagnostic viewpoint, this difference disappears after a single treatment with temozolomide (TMZ). The second example illustrates the use of an exogenous paraCEST agent as a glucose sensor (54).

One can see from equation [5] that CEST contrast ($M_z/M_o$) depends upon some of the same parameters as those governing $T_1$-based agents including concentration, *q* (number of exchanging protons), the $T_1$ of bulk water protons, and $\tau_m$, the water proton exchange lifetime. The basic rule that governs whether a molecule can act as a CEST contrast agent is that the chemical shift between the exchanging protons and water protons ($\Delta\omega$) must differ and the proton exchange rate must be slow compared to the frequency difference, $\Delta\omega > k_{ex}$ (or alternatively, $\Delta\omega \bullet \tau_m > 1$). Given that increases with $B_0$ while $k_{ex}$ is independent of field strength, this also means that many more molecules (both endogenous and exogenous) should be amenable to CEST detection at higher imaging fields compared to lower imaging fields.

## 2.3. Methods to optimize the $r_1$ relaxivity of $Gd^{3+}$ complexes

Most clinically approved contrast agents have $r_1$ relaxivity values in the range of 4–5 $mM^{-1}s^{-1}$ (Table 1). To increase the relaxivity of a $Gd^{3+}$-based CA to the theoretical maximum of 40 $mM^{-1}s^{-1}$ at 1.5 T or 100 $mM^{-1}s^{-1}$ at 9.4T (55), scientists have focused on optimizing one of three parameters: *q*, $\tau_m$, or $\tau_R$. However, several parameters depend on the strength of magnetic field so this should be considered when designing a new CA.

**3.3.1 Modulating the hydration number, q—**According to the Solomon–Bloembergen –Morgan (SBM) theory the proton relaxivity is directly proportional to the number of water molecules coordinated to the paramagnetic center (25). This in principle means that one could simply increase the number of water molecules bound to $Gd^{3+}$ and the $r_1$ relaxivity should increase proportionally. In the discussion that follows, we will present perspectives largely based on our own experiences with GdDOTA, although the principles are broadly applicable to other non-macrocyclic ligands as well. In aqueous media, GdDOTA exists as a mixture of two nona-coordinated isomers, a twisted square antiprism (TSAP) and a square antiprism (SAP), where $Gd^{3+}$ sits in the center with the eight corners of the anticube occupied by the four nitrogen atoms and four carboxylate oxygen atoms of the ligand. The ninth position above the plane of the four oxygen atoms is occupied by a water molecule. If one were to remove one acetate group from GdDOTA, this would open up another coordination position for a second water molecule to coordinate to the $Gd^{3+}$ ion. This "extra" coordination position for water increases the $r_1$ from 4.3 $mM^{-1}s^{-1}$ (GdDOTA) to 6.2 $mM^{-1}s^{-1}$ (GdDO3A) (56) (Figure 4A). This is not a doubling of $r_1$ as one might have anticipated because about 50% of the GdDOTA $r_1$ arises from outer-sphere relaxation. If one were to remove yet another acetate group to produce GdDO2A (Figure 4A), *q* does increase to 3 but the $r_1$ relaxivity increases to only 6.5 $mM^{-1}s^{-1}$. This indicates that other factors such as overall charge on the complex ($GdDOTA^-$, $GdDO3A^0$, $GdDO2A^+$) also play a role. It has also been shown that the thermodynamic stability and kinetic inertness of

GdDO2A (log $K_{st}$ = 13.6) (57) is substantially worse than that of GdDO3A (log $K_{st}$ = 21.0) (56) or GdDOTA (Table 1) so the *q*=3 complex is simply too unstable for *in vivo* applications.

**3.3.2 Modulating water exchange, $\tau_m$—**The rate of water exchange between the inner-sphere of a metal ion and bulk water is quite important in the design of the most efficient CA for MRI, whether it be a $Gd^{3+}$-based $T_1$-agent or a CEST agent (58). For those agents approved for clinical use many years ago, the rate of water exchange was not an important consideration during their development for a couple of reasons. First, water exchange rates had not been reported for any of the $Gd^{3+}$ complexes at that time but it was known that water exchange in the free $Gd^{3+}$ ion ($Gd(H_2O)_8^{3+}$) was extremely rapid (1.2 ns) (59). Thus, it was natural to assume that water exchange in all of the various $Gd^{3+}$ chelates under development would be equally fast.

Second, SBM theory predicts that the $r_1$ relaxivity of rapidly tumbling, low molecular weight $Gd^{3+}$complexes is not very sensitive to the rate of water exchange over a broad range of $\tau_m$ values. It can be seen by the data in Table 1 that $\tau_m$ varies by nearly 20-fold for the first six compounds listed while $r_1$ changes by less than 20%. However, as one begins to think about targeting one of these small molecule agents to a larger biological structure such as a cell receptor or specific protein for imaging purposes, then $\tau_m$ becomes critically important because the maximum $r_1$ one can achieve by slowing molecular tumbling depends heavily upon the water exchange rate. SBM theory predicts that for a $Gd^{3+}$-based $T_1$ agent to achieve its highest $T_1$ sensitivity (maximum $r_1$), the optimal bound water lifetime is about 10 ns at 1.5T (25). As one can see in Table 1, the bound water lifetime for each of the current clinical agents is too long to achieve optimal $r_1$ when bound to a biological target. Various strategies to modify $\tau_m$ have been discussed in the literature (60) but we will briefly describe those factors that can be manipulated by basic ligand design. These effects can generally be attributed to stabilization or destabilization of intermediates involved in the water exchange mechanism and/or changes in the population of various CA isomers present in solution.

**3.3.2.1 Strategies to increase the rate of water exchange:** Increasing the steric hindrance around the $Ln^{3+}$ coordination sphere forces the bound water molecule to reside, on average, further away from the $Ln^{3+}$ ion thereby making it easier for the water molecule to leave the coordination sphere and mix with the much larger pool of bulk water molecules. This is exemplified by a comparison of bound water lifetimes in the $Gd^{3+}$ complexes of DOTA (macrocycle containing 12 atoms, $\tau_m$ = 122 ns) with TRITA (macrocycle containing 13 atoms, $\tau_m$ = 3.7 ns) (61) or DO3A-N-prop (one acetate replaced by a propionate, $\tau_m$ = 16.4 ns) (62) (see Figure 4B to inspect the ligand structures discussed in this section). While GdDO3A-N-prop displays a near optimal $\tau_m$ value, the kinetic stability of the complex is somewhat compromised compared to GdDOTA. This effect is even more pronounced in GdTRITA, which has a relatively poor kinetic stability ($k_1$ = 0.21 $M^{-1}s^{-1}$) (63). Adding a charged group to the ligand also has an effect on water exchange. For example, addition of an amino group to the propyl side-chain of DO3A-N-prop to yield DO3A-α-amino-prop results in a dramatic shortening of the bound water lifetime (25 ns) in the resulting $Gd^{3+}$

complex (64). On the other hand, when a negatively charged acetate group is added to DO3A-N-prop to form DOTA-SA, the water exchange rate in the corresponding $Gd^{3+}$ complex becomes slower (159 ns) (65) compared to the DO3A-α-amino-prop derivative. An interesting feature of the GdDOTA-SA complex is that its rotational correlation time is slower than GdDOTA (125 ps versus 53 ps, respectively) which must be attributed to the additional negative charge of the extra carboxylate. It is believed that this carboxylate may assemble extra water molecules in the second coordination sphere which makes the effective molecular weight of the complex larger and hence molecular rotation becomes slower. GdDOTA-SA also has the highest thermodynamic stability (log $K_{st}$ = 27.2) reported to date for DOTA-like complexes and this again can be attributed to the excess negative charge (65). Addition of a bulky group onto the α position of an acetate side-chain also has an impact on water exchange. For example, when four methyl groups are introduced, one per acetate, as in GdDOTMA, the population of coordination isomers changes from favoring the SAP isomer in GdDOTA to favoring the TSAP isomer in GdDOTMA. Given that water exchange has been observed to be ~50-fold faster in TSAP isomers compared with SAP isomers, it is not surprising to find that the measured water exchange lifetime is faster in GdDOTMA ($_M$ = 85 ns) than in GdDOTA ($_M$ = 122 ns).

**3.3.2.2 Strategies to decrease the rate of water exchange:** Unlike next generation $Gd^{3+}$-based $T_1$ agents that must be optimized for faster water exchange kinetics, next generation CEST require just the opposite, they must be optimized for slow-to-intermediate water exchange. One effective way to slow water exchange in DOTA-based complexes is to replace the negatively carboxylate groups (-$COO^-$) with neutral amide groups (-CONHR). Given that the oxygen atom of an amide group is less basic than an oxygen atom of carboxylate, a single amide substitution can have a dramatic effect on the rate of water exchange. For example, water exchange in the mono-amide complex, GdDOTA-1-Bz-$NO_2$, is about 5-fold slower ($\tau_m$ = 625 ns) than that in GdDOTA. Typical GdDOTA-bis-amide complexes display even slower water exchange as evidenced by the $\tau_m$ value reported for GdDOTA-2DMA (811 ns) (66) while GdDOTA-tetra-amide complexes such as GdDOTAM have bound water lifetimes extending into the several μs range (19 μs) (67). It has also been shown that the bound water lifetime decreases with an increase in the number of methyl substituents on the amide nitrogen (compare GdDTMA ($\tau_m$ = 17 μs) *versus* GdDOTTA ($\tau_m$ = 7.8 μs) (67). This indicates that the increased steric bulkiness provided by the two methyl substituents can be used to fine-tune water exchange rates in such complexes.

**3.3.3 Modulating the rotational correlation time, $\tau_R$—**SBM theory for paramagnetic relaxation predicts that reducing the rate of molecular tumbling (making $\tau_R$ longer) will enhance the relaxivity of a $T_1$ contrast agent. This fundamental concept has been widely used in the design of biologically responsive agents. $\tau_R$ can be made longer either by coupling the molecular motion of the agent to that of a larger structure such as binding to a protein or by increasing the molecular size of the agent itself. Binding of an agent to a protein is the principle behind gadofosveset trisodium, a low molecular weight complex that binds reversibly to human serum albumin (HSA). In the basic design, the agent is covalently attached through a linker to a unit capable of binding to HSA, thereby slowing molecular reorientation of the agent itself (68). The nature of the linker and the conformational

arrangement of the agent receptor complex determine the efficacy of the construct in slowing molecular motion and thereby enhancing $r_1$ relaxivity. If the linker is flexible (such as an alkyl chain), then local molecular motion of the agent might dominate $\tau_R$ even with the agent bound at its target. A partial solution to this problem is to use a rigid linker but even then, the impact on $\tau_R$ will still depend on the conformation attained by the agent when interacting with its macromolecular target. This interaction could in principle increase or decrease the rate of water exchange or perhaps even block water access to the agent entirely. Both scenarios have been observed experimentally. Furthermore, challenges in design are reflected in the behavioral variance that was noted when MS-325 derivatives with different hydration numbers (q = 0, 1 and 2) (Fig. 4C) were prepared and characterized in absence and presence of HSA (69). In this example, an agent with optimal water exchange properties in aqueous buffer showed a lower than expected increase in $r_1$ when the agent was bound to the protein target HSA, highlighting the complex interactions of water exchange and/or local motional flexibility.

In a second example, two DOTMA-like derivatives (see BIP-S-NB-3R-DOTMA and BIP-S-NB-3S-DOTMA structures in Fig. 4C) were modified with a hydrophobic biphenyl unit for binding to HSA. The solution structure of GdBIP-S-NB-3R-DOTMA was locked into the SAP geometry while GdBIP-S-NB-3S-DOTMA was locked into the TSAP geometry. These complexes had bound water lifetimes of 70 and 8 ns and $r_1$ values of 10.7 and 9.0 $mM^{-1}s^{-1}$, respectively, in aqueous buffer and 46.8 and 37.6 $mM^{-1}s^{-1}$ when bound to HSA (70). This was an unexpected result since SBM theory predicts that the isomer with the fastest water exchange would show the largest increase in relaxivity upon binding to HSA. Further investigations showed no change in water exchange kinetics for both compounds when bound to the protein relative to their unbound state so the larger increase in relaxivity of the SAP isomer was attributed to a difference of hydration states between the isomers when bound to the protein (less water access with the TSAP structure bound to protein). This example again illustrates the difficulty of designing a MR agent that retains optimal water exchange kinetics when bound to a protein target.

These examples highlight some challenges one faces when designing a single monomeric MR agent (one $Gd^{3+}$ per molecule) that can achieve an optimal $r_1$ (<40 $mM^{-1}s^{-1}$) value when bound to a protein target. Another approach may be to attach a few $Gd^{3+}$ chelates each having a non-optimized $r_1$ to create a multimeric scaffold (e.g., polymers, hyperbranched polymers, dendrimers) or nanoparticle (71). Gadomer-17 is a good example of such a multimeric system (Figure 4D). Gadomer-17 consists of a trimesoyltriamide central core further functionalized with a second generation lysine dendron having 24 terminal amino residues (α and ε). Addition of 24 GdDOTA-monoamide groups to this small dendron yielded a molecule with a MW of 17,500, large enough to be retained in the vascular space somewhat longer than an extracellular agent such as gadopentetate dimeglumine (GdDTPA) or gadoteridol (GdHP-DO3A) so can be considered a blood pool agent with a distribution similar to that of MS-325. However, unlike MS-325 which has a $r_1$ of 46.1 $mM^{-1}s^{-1}$ when bound to albumin, the $r_1$ of Gadomer-17 is only 16.4 $mM^{-1}s^{-1}$. Why might this be so? First, the single amide bond in each GdDOTA-monoamide unit of Gadomer-17 has less than optimal water exchange ($\tau_M$ = 1 μs) and, second, the unrestricted motional flexibility of each

appended GdDOTA-monoamide unit limits the agent from "feeling" the impact of being part of a larger molecule. So, even though the rotational correlation time of the dendron backbone structure is reasonably long (3.05 ns), the local rotational correlation time felt by each $Gd^{3+}$ atom is only about 760 ps. This later value is about 3.5 times longer than a typical low MW $Gd^{3+}$ chelate (211 ps for GdDOTA-1-Bz-$NO_2$) but nonetheless not long enough for the agent to experience the full advantages of slow rotation (72). This combination of factors, a non-optimal water exchange rate and relatively fast internal rotational motion combine to limit the relaxivity of the dendron (16.4 $mM^{-1}s^{-1}$, 25°C, 0.47T). Subsequent designs have solved these limitations using various approaches as illustrated in Figure 5 (55) (69)(73). In these designs, the selection of the linker is important not only to give rigidity or mobility to the final construct but also to minimize negative effects on the binding affinity to the receptor.

## 3. Current clinical examples of the use of MR contrast agents

Eleven intravenously administered MR contrast agents (74) have been approved for clinical use by the US FDA since gadopentetate dimeglumine (GdDTPA) was first introduced in 1986. The most commonly used in clinical practice are extracellular agents that have no specific tissue biodistribution (an exception is cartilage where the distribution of an anionic agents is lower than a neutral agent because of repulsion from negatively charged glycosoaminoglycans in the tissue) and are quickly eliminated in well-functioning kidneys ($t_{1/2}$~ 1.5 hrs). Elimination times increase with renal impairment ($t_{1/2}$~ 4–8 hrs for moderately impaired subjects and up to 18–34 hrs for severely impaired patients) (75). The original application of these agents was to facilitate the detection of central nervous system neoplasms (Figure 6). This was followed by other CNS applications such as tumor grading (Figure 7) and applications geared towards improving the detection and later characterization of tumors throughout the body (76). Soon after, the first class of organ specific contrast agents emerged with the development of mangafodipir trisodium (Mn-DPDP), Gd-BOPTA and later Gd-EOB-DTPA as hepatobiliary MRI CAs (77). The two $Gd^{3+}$-based agents are DTPA derivatives containing one lipophilic residue attached to one acetate side-arm. This feature targets each agent to an organic anion transporter in the sinusoidal plasma membrane of the hepatocyte (Figure 8). The amount of agent taken up by liver varies considerably even though the chemistry of the lipophilic groups do not differ substantially (~4% for Gd-BOPTA and 50% for Gd-EOB-DTPA). Both agents have slightly higher relaxivities *in vivo* compared to GdDTPA due to weak binding interactions with human serum albumin (HSA). These slightly higher relaxivities allow these agents to be used at somewhat lower doses which brings potential safety benefits for the patient (78). A recently approved CA widely known as gadofosveset trisodium and now sold under the generic name GdMS-325 (Figure 10) binds reversibly to serum albumin ($K_D$ = 85 μM) but has minimal hepatic clearance. MS-325 has a higher affinity for HSA compared to Gd-BOPTA and Gd-EOB-DTPA due to the more lipophilic nature of the biphenylcyclohexyl group. This results in a long plasma lifetime (18.5 hrs) and higher relaxivity due to an increase in $\tau_R$ (Table 1).

The recognition of nephrogenic system fibrosis (NSF) as a disease associated with administration of gadolinium chelates has resulted in more awareness of the importance of

kinetic stability in choosing the most appropriate CA for clinical use. The incidence of NSF has been shown to be most highly associated with use of the nonionic linear agents gadodiamide and gadoversetamide (GdDTPA-BMA and GdDTPA-BMEA), intermediate with the ionic linear agent gadopentetate dimeglumine (GdDTPA), and lowest with the macrocyclic agents gadoterate meglumine, gadoteridol, gadobutrol (GdDOTA, GdHP-DO3A and GdDO3A-butrol). In clinical practice, the choice of gadolinium based contrast agents is a balanced consideration between a given agent's safety, tolerance, efficacy and cost. As described in this review, the chemical and physical considerations support the use of the macrocyclic agents. This is especially pertinent in those patients with a glomerular filtration rate (GFR) <30 mL/min. Such individuals are best served when identified before contrast administration either by measuring serum creatinine or by using a questionnaire to identify individuals at risk (79). The use of macrocyclic agents has expanded worldwide in the last decade and in conjunction with the judicious use of gadolinium protocols in patients with known or suspected renal insufficiency, the incidence of NSF has been substantially reduced (80,81).

## 4. Examples of next generation MR contrast agents

The first example of a "smart" or "responsive" MRI contrast agent reported in 1997 (82) was designed to detect the presence of β-D-galactosidase, an enzyme commonly used in molecular biology as a biomarker of gene expression. This first design was based on an increase water access to the inner coordination sphere of the $Gd^{3+}$ (an increase in $q$) by removing the blocking group β-D-galactose from one face of a GdDO3A chelate (Figure 10A). It was thought that the sugar would at least partially block access of water molecules to the $Gd^{3+}$ to yield a $q = 0$ "off" state and the agent could be turned "on" by cleavage of the sugar unit to allow full access of water ($q = 1$) to the $Gd^{3+}$ ion. This first report stimulated many other responsive agent designs based on a change in $q$. A few examples include agents that respond to $Ca^{2+}$, $Cu^{2+}$, $Cu^{+}$, $Zn^{2+}$ (83)(84)(85), pH, and tissue redox (86). Unfortunately, very few of these responsive agents have been applied *in vivo* so we will limit our discussion here to some of those which have been demonstrated to work *in vivo*. This will give the reader a sense of potential clinical applications of responsive MRI agents while appreciating their limitations as well.

Another responsive contrast agent design for imaging enzyme activity *in vivo* is exemplified by agents designed to respond to myeloperoxidase (MPO) activity based on slowing molecular rotation. MPO is an important marker of vascular disease in humans since it is highly secreted by neutrophils and macrophages in advanced human atherosclerotic plaque. MPO activity *in vivo* has a clear outcome-predictive value in several cardiovascular diseases, including myocardial infarction and ischemic stroke (87). MPO-responsive agents take advantage of the known polymerization activity of the enzyme on tyrosine-like derivatives. The basic idea was to functionalize a stable GdDO3A complex with a unit that could be polymerized by MPO, converting it from a low MW, low $r_1$ agent into a higher MW, higher $r_1$ polymerized form. Among the first reported MPO-responsive agents was a GdDO3A derivative containing a 5-hydroxytryptamide unit (Figure 10B) (88). However, *in vivo* application of this agent has not been reported likely due to a modest increase in relaxivity that occurs upon polymerization. This can be attributed to the flexibility of the

linker that binds the complex in the polymeric chain. An improved MPO agent was subsequently developed which consists of DTPA derivative having two 5-hydroxytryptamide units (Figure 10B) which should in principle promote cross-linking of the polymer matrix to increase the rigidity of the paramagnetic complex (89) and thereby yield a greater increase in $r_1$ relaxivity. The utility of this GdDTPA-bis-5-hydroxytryptamide to image MPO activity *in vivo* was demonstrated by imaging mice 2 days after coronary ligation before and after intravenous injection of GdDTPA-bis-5-hydroxytryptamide (or GdDTPA as control) at 0.3 mmol/Kg dose. Mice injected with the MPO-responsive agent showed sustained contrast enhancement in the injured myocardium at 120 min after injection while image contrast in control mice returned to baseline after 60 min. The prolonged enhancement of the MPO-responsive agent was attributed to cross-linking of the agent to surrounding matrix proteins (90).

Responsive MRI agents have also been designed to target specific proteins known to be overexpressed in certain pathologies. Among the first examples of these include fibrin and collagen. Thrombosis or blood clot formation is the underlying pathology in myocardial infarction, ischemic stroke, pulmonary embolism, and deep vein thrombosis, conditions that affect millions of individuals worldwide. In the clotting process, activated platelets and fibrin form a hemostatic plug. Fibrin is formed when the enzyme thrombin cleaves the fibrin peptides on circulating fibrinogen protein enabling end-to-end polymerization of the fibrinogen moieties. The resultant fibrin mesh is further stabilized with cross-linking induced by the enzyme, Factor XIII. Fibrin is an excellent target for MR detection since it is present in arterial and venous clots at high concentrations (20–100 μM) but is not found in plasma. One of the most promising fibrin-responsive agents is EP-2104R, a cyclic peptide with four appended GdDOTA complexes (Figure 11A). EP-2104R, first developed by EPIX Medical has a 3-fold higher $r_1$ relaxivity (10.1 $mM^{-1}s^{-1}$, 1.5T, 37°C, pH 7.4) per $Gd^{3+}$ ion over GdDOTA, largely reflecting the higher molecular weight of agent. EP-2104R has an acceptable binding affinity to human fibrin ($K_D \approx$ 1.7 μM) and shows an 80% increase in relaxivity (17.9 $mM^{-1}$ $s^{-1}$ per Gd at 1.5T, 37°C, pH 7.4) when bound to fibrin. This enhanced relaxivity can be attributed largely to slowing of molecular rotational motion when the complex is bound to largely immobile fibrin clot. EP-2104R is effective at providing positive contrast enhancement in preclinical models of carotid artery, coronary artery, atrial and cerebral venous sinus, thrombosis and pulmonary embolism (91). Due to its success in pre-clinical tests, EP-2104R was the first responsive contrast agent to advance to clinical trials. A similar approach has been used to create a collagen I specific MRI contrast agent, which could be applied for screening of chronic diseases of the heart, kidney, liver, lungs, or vasculature. (Figure 11B) (92).

$Gd^{3+}$-based agents that bind to human serum albumin (HSA) and show an increase $r_1$ relaxivity in response to a secondary physiological signal have also emerged. The first example of this is kind was GdDOTA-diBPEN, a $Zn^{2+}$ responsive agent that binds to HSA only after two $Zn^{2+}$ ions are first bound to the agent (Figure 12I) (93). GdDOTA-diBPEN-$(Zn)_2$ displays a large change in relaxivity when fully bound to HSA (6.6 ± 0.1 to 17.4 ± 0.5 $mM^{-1}$ $s^{-1}$, 37°C, pH 7.6) and this effect has been used to monitor $Zn^{2+}$ release from pancreatic β-cells that accompanies insulin secretion. This change in relaxivity has important

implications for use in the clinic because one could administer the CA at such a low dose that it is not detected when exposed to physiological levels of $Zn^{2+}$ (total $Zn^{2+}$ concentration in blood is ~15 μM) but is detected whenever the local $Zn^{2+}$ concentration is high. This concept was first evaluated in control mice, in diet-induced obese mice, and in streptozotocin-treated "diabetic" by administering 0.03 mmol/Kg of GdDOTA-diBPEN (Figure 12II). Contrast enhancement was not observed in regions of pancreas prior to injection of glucose but was detected after stimulation of insulin secretion by glucose. The image intensity changes observed in regions of the pancreas differed among control mice, obese mice (expanded β-cell mass) and STZ treated mice (mice lacking β-cells) as expected for animals with different β-cell function and likely β-cell mass (although this was not measured) (94). It is known that $Zn^{2+}$ ions are required for proper storage of insulin in β-cells and that $Zn^{2+}$ is released from β-cells during exocytosis of insulin so it appears that this responsive agent may prove useful as a biomarker of β-cell function *in vivo*. Such MRI technology could prove extremely useful for monitoring β-cell function in response to new drugs currently under development for improving insulin responsiveness in Type 2 diabetic patients.

## 5. Summary

MR contrast agents continue to play an important role in the arsenal of tools available to the clinical radiologist. Although many of the CA introduced over the past 27 years have similar features in terms of $r_1$ relaxivity and size, some are ionic while others are non-ionic, some have appended organic groups which increase the relative uptake in liver, but most distribute quickly into all extracellular space. Gadofosveset trisodium (MS-325) is unique among them in that it was designed to have a modest affinity for serum albumin so that it would remain in the vascular space for an extended period of time. Newer agents that respond to some specific biological function hold great promise for improving diagnostic content in medical imaging. However, the current regulatory environment challenges the successful and timely implementation of new agents into clinical practice. Meanwhile, scientists around the world have been busy unraveling the fundamental physical and chemical limitations of current CA and publishing newer designs capable of providing much more specific biological information. Many labs have demonstrated that the rate of water exchange on-and-off a CA is the key physical parameter for the successful development of new agents having the highest sensitivity for detection by MRI. Given the recent exciting advances in biologically responsive $Gd^{3+}$-based $T_1$ agents and $Eu^{3+}$-based paraCEST agents, it is our hope that many new agents will become part of the arsenal of tools available to the radiologist in the coming years.

## Acknowledgements

ADS wishes to acknowledge grant support from the NIH (CA-115531, DK-095416, EB-015908, and EB-04582), the ADA (17-12--IN-42-01), and the Robert A. Welch Foundation (AT-584) during the writing of this review.

## REFERENCES

1. Lauffer RB. Paramagnetic metal complexes as water proton relaxation agents for NMR imaging: theory and design. Chem. Rev. 1987; 87:901–927.

2. Caravan P, Ellison JJ, McMurry TJ, Lauffer RB. Gadolinium(III) Chelates as MRI Contrast Agents: Structure, Dynamics, and Applications. Chem. Rev. 1999; 99:2293–2352. [PubMed: 11749483]
3. Reilly RF. Risk for Nephrogenic Systemic Fibrosis with Gadoteridol (ProHance) in Patients Who Are on Long-Term Hemodialysis. Clin J Am Soc Nephrol. 2008; 3:747–751. [PubMed: 18287249]
4. Wiginton CD, Kelly B, Oto A, Jesse M, Aristimuno P, Ernst R, Chaljub G. Gadolinium-Based Contrast Exposure, Nephrogenic Systemic Fibrosis, and Gadolinium Detection in Tissue. Am J Roentgenol. 2008; 190:1060–1068. [PubMed: 18356456]
5. Bhave G, Lewis JB, Chang SS. Association of Gadolinium Based Magnetic Resonance Imaging Contrast Agents and Nephrogenic Systemic Fibrosis. J. Urol. 2008; 180:830–835. [PubMed: 18635232]
6. Yantasee W, Fryxell GE, Porter GA, Pattamakomsan K, Sukwarotwat V, Chouyyok W, Koonsiripaiboon V, Xu J, Raymond KN. Novel sorbents for removal of gadolinium-based contrast agents in sorbent dialysis and hemoperfusion: Preventive approaches to nephrogenic systemic fibrosis. Nanomedicine Nanotechnol. Biol. Med. 2010; 6:1–8.
7. Rohrer M, Bauer H, Mintorovitch J, Requardt M, Weinmann H-J. Comparison of magnetic properties of MRI contrast media solutions at different magnetic field strengths. Invest. Radiol. 2005; 40:715–724. [PubMed: 16230904]
8. Chan KWY, Wong WT. Small molecular gadolinium(III) complexes as MRI contrast agents for diagnostic imaging. Coord. Chem. Rev. 2007; 251:2428–2451.
9. Idée JM, Port M, Robic C, Medina C, Sabatou M, Corot C. Role of thermodynamic and kinetic parameters in gadolinium chelate stability. J. Magn. Reson. Imaging. 2009; 30:1249–1258. [PubMed: 19938037]
10. Brücher, E.; Tircsó, G.; Baranyai, Z.; Kovács, Z.; Sherry, AD. Stability and Toxicity of Contrast Agents. In: Merbach, A.; Helm, L.; Tóth, É., editors. The Chemistry of Contrast Agents in Medical Magnetic Resonance Imaging. John Wiley & Sons, Ltd; 2013. p. 157-208.
11. Wedeking P, Kumar K, Tweedle MF. Dissociation of gadolinium chelates in mice: Relationship to chemical characteristics. Magn. Reson. Imaging. 1992; 10:641–648. [PubMed: 1501535]
12. Brücher, E. Kinetic Stabilities of Gadolinium(III) Chelates Used as MRI Contrast Agents. In: Krause, PDW., editor. Contrast Agents I. Topics in Current Chemistry. Springer Berlin Heidelberg; 2002. p. 103-122.
13. Aime S, Botta M, Panero M, Grandi M, Uggeri F. Inclusion complexes between β-cyclodextrin and β-benzyloxy-α-propionic derivatives of paramagnetic DOTA- and DPTA-Gd(III) complexes. Magn. Reson. Chem. 1991; 29:923–927.
14. Martell, AE.; Smith, RM. Critical Stability Constants: Inorganic Complexes. Plenum Press; 1976.
15. Kumar K, Chang CA, Francesconi LC, Dischino DD, Malley MF, Gougoutas JZ, Tweedle MF. Synthesis, Stability, and Structure of Gadolinium(III) and Yttrium(III) Macrocyclic Poly(amino carboxylates). Inorg. Chem. 1994; 33:3567–3575.
16. Toth E, Brucher E, Lazar I, Toth I. Kinetics of Formation and Dissociation of Lanthanide(III)-DOTA Complexes. Inorg. Chem. 1994; 33:4070–4076.
17. Powell DH, Dhubhghaill OMN, Pubanz D, Helm L, Lebedev YS, Schlaepfer W, Merbach AE. Structural and Dynamic Parameters Obtained from 17O NMR, EPR, and NMRD Studies of Monomeric and Dimeric Gd3+ Complexes of Interest in Magnetic Resonance Imaging: An Integrated and Theoretically Self-Consistent Approach1. J. Am. Chem. Soc. 1996; 118:9333–9346.
18. Cacheris WP, Quay SC, Rocklage SM. The relationship between thermodynamics and the toxicity of gadolinium complexes. Magn. Reson. Imaging. 1990; 8:467–481. [PubMed: 2118207]
19. Shukla R, Fernandez M, Pillai RK, Ranganathan R, Ratsep PC, Zhang X, Tweedle MF. Design of conformationally rigid dimeric MRI agents. Magn. Reson. Med. Off. J. Soc. Magn. Reson. Med. Soc. Magn. Reson. Med. 1996; 35:928–931.
20. Tóth É, Király R, Platzek J, Radüchel B, Brücher E. Equilibrium and kinetic studies on complexes of 10-[2,3-dihydroxy-(1-hydroxymethyl)-propyl]-1,4,7,10-tetraazacyclododecane-1,4,7-triacetate. Inorganica Chim. Acta. 1996; 249:191–199.

21. Vogler H, Platzek J, Schuhmann-Giampieri G, Frenzel T, Weinmann H-J, Radüchel B, Press W-R. Pre-clinical evaluation of gadobutrol: a new, neutral, extracellular contrast agent for magnetic resonance imaging. Eur. J. Radiol. 1995; 21:1–10. [PubMed: 8654452]
22. Baranyai Z, Brücher E, Iványi T, Király R, Lázár I, Zékány L. Complexation Properties of N,N′,N″,N‴-[1,4,7,10-Tetraazacyclododecane-1,4,7,10-tetrayltetrakis(1-oxoethane-2,1-diyl)]tetrakis[glycine] (H4dotagl). Equilibrium, Kinetic, and Relaxation Behavior of the Lanthanide(III) Complexes. Helv. Chim. Acta. 2005; 88:604–617.
23. Soesbe TC, Ratnakar SJ, Milne M, Zhang S, Do QN, Kovacs Z, Sherry AD. Maximizing T2-exchange in Dy3+DOTA-(amide) X chelates: Fine-tuning the water molecule exchange rate for enhanced T2 contrast in MRI. Magn. Reson. Med. 2014; 71:1179–1185. [PubMed: 24390729]
24. Rothermel GL Jr, Rizkalla EN, Choppin GR. The kinetics of exchange between a lanthanide ion and the gadolinium complex of N,N″-bis(2-methoxyethylamide-carbamoylmethyl)-diethylenetriamine-N,N′,N″-triacetate. Inorganica Chim. Acta. 1997; 262:133–138.
25. Merbach, AE.; Helm, L.; Toth, E. The Chemistry of Contrast Agents in Medical Magnetic Resonance Imaging. 2nd ed.. Wiley; 2013.
26. Caravan P, Comuzzi C, Crooks W, McMurry TJ, Choppin GR, Woulfe SR. Thermodynamic stability and kinetic inertness of MS-325, a new blood pool agent for magnetic resonance imaging. Inorg. Chem. 2001; 40:2170–2176. [PubMed: 11304163]
27. Baranyai Z, Pálinkás Z, Uggeri F, Brücher E. Equilibrium Studies on the Gd3+, Cu2+ and Zn2+ Complexes of BOPTA, DTPA and DTPA-BMA Ligands: Kinetics of Metal-Exchange Reactions of [Gd(BOPTA)]2–. Eur. J. Inorg. Chem. 2010; 2010:1948–1956.
28. Baranyai Z, Pálinkás Z, Uggeri F, Maiocchi A, Aime S, Brücher E. Dissociation Kinetics of Open-Chain and Macrocyclic Gadolinium(III)-Aminopolycarboxylate Complexes Related to Magnetic Resonance Imaging: Catalytic Effect of Endogenous Ligands. Chem. – Eur. J. 2012; 18:16426–16435. [PubMed: 23139193]
29. Rofsky NM, Sherry AD, Lenkinski RE. Nephrogenic Systemic Fibrosis: A Chemical Perspective. Radiology. 2008; 247:608–612. [PubMed: 18487530]
30. Silverio S, Torres S, Martins AF, Martins JA, Andre JP, Helm L, Prata MIM, Santos AC, Geraldes CFGC. Lanthanide chelates of (bis)-hydroxymethyl-substituted DTTA with potential application as contrast agents in magnetic resonance imaging. Dalton Trans. 2009:4656–4670. [PubMed: 19513474]
31. Wang X, Jin T, Comblin V, Lopez-Mut A, Merciny E, Desreux JF. A kinetic investigation of the lanthanide DOTA chelates. Stability and rates of formation and of dissociation of a macrocyclic gadolinium(III) polyaza polycarboxylic MRI contrast agent. Inorg. Chem. 1992; 31:1095–1099.
32. Aime S, Calabi L, Cavallotti C, Gianolio E, Giovenzana GB, Losi P, Maiocchi A, Palmisano G, Sisti M. [Gd-AAZTA]-: a new structural entry for an improved generation of MRI contrast agents. Inorg. Chem. 2004; 43:7588–7590. [PubMed: 15554621]
33. Datta A, Raymond KN. Gd-hydroxypyridinone (HOPO)-based high-relaxivity magnetic resonance imaging (MRI) contrast agents. Acc. Chem. Res. 2009; 42:938–947. [PubMed: 19505089]
34. Schellenberger EA, Högemann D, Josephson L, Weissleder R. Annexin V-CLIO: a nanoparticle for detecting apoptosis by MRI. Acad. Radiol. 2002; 9(Suppl 2):S310–311. [PubMed: 12188257]
35. Yeh T-C, Zhang W, Ildstad ST, Ho C. In Vivo Dynamic MRI Tracking of Rat T-Cells Labeled with Superparamagnetic Iron-Oxide Particles. Magn. Reson. Med. 1995; 33:200–208. [PubMed: 7707910]
36. Na HB, Song IC, Hyeon T. Inorganic Nanoparticles for MRI Contrast Agents. Adv. Mater. 2009; 21:2133–2148.
37. Bannas P, Graumann O, Balcerak P, Peldschus K, Kaul MG, Hohenberg H, Haag F, Adam G, Ittrich H, Koch-Nolte F. Quantitative magnetic resonance imaging of enzyme activity on the cell surface: in vitro and in vivo monitoring of ADP-ribosyltransferase 2 on T cells. Mol. Imaging. 2010; 9:211–222. [PubMed: 20643024]
38. Ittrich H, Peldschus K, Raabe N, Kaul M, Adam G. Superparamagnetic iron oxide nanoparticles in biomedicine: applications and developments in diagnostics and therapy. RöFo Fortschritte Auf Dem Geb. Röntgenstrahlen Nukl. 2013; 185:1149–1166.

39. Koenig SH, Kellar KE. Theory of 1/T1 and 1/T2 NMRD profiles of solutions of magnetic nanoparticles. Magn. Reson. Med. 1995; 34:227–233. [PubMed: 7476082]
40. Roch A, Muller RN, Gillis P. Theory of proton relaxation induced by superparamagnetic particles. J. Chem. Phys. 1999; 110:5403–5411.
41. Zhao Z, Zhou Z, Bao J, et al. Octapod iron oxide nanoparticles as high-performance T2 contrast agents for magnetic resonance imaging. Nat. Commun. 2013; 4:1–7.
42. Choi JH, Nguyen FT, Barone PW, Heller DA, Moll AE, Patel D, Boppart SA, Strano MS. Multimodal Biomedical Imaging with Asymmetric Single-Walled Carbon Nanotube/Iron Oxide Nanoparticle Complexes. Nano Lett. 2007; 7:861–867. [PubMed: 17335265]
43. Pereira GA, Ananias D, Rocha J, Amaral VS, Muller RN, Elst LV, Tóth É, Peters JA, Geraldes CFGC. NMR relaxivity of Ln3+-based zeolite-type materials. J. Mater. Chem. 2005; 15:3832–3837.
44. Pereira GA, Peters JA, Almeida Paz FA, Rocha J, Geraldes CFGC. Evaluation of [Ln(H2cmp)(H2O)] Metal Organic Framework Materials for Potential Application as Magnetic Resonance Imaging Contrast Agents. Inorg. Chem. 2010; 49:2969–2974. [PubMed: 20151642]
45. Carné-Sánchez A, Bonnet CS, Imaz I, Lorenzo J, Tóth É, Maspoch D. Relaxometry Studies of a Highly Stable Nanoscale Metal-Organic Framework Made of Cu(II), Gd(III), and the Macrocyclic DOTP. J. Am. Chem. Soc. 2013; 135:17711–17714. [PubMed: 24215474]
46. Viswanathan S, Kovacs Z, Green KN, Ratnakar SJ, Sherry AD. Alternatives to gadolinium-based metal chelates for magnetic resonance imaging. Chem. Rev. 2010; 110:2960–3018. [PubMed: 20397688]
47. Pouliquen D, Perdrisot R, Ermias A, Akoka S, Jallet P, Le Jeune JJ. Superparamagnetic iron oxide nanoparticles as a liver MRI contrast agent: Contribution of microencapsulation to improved biodistribution. Magn. Reson. Imaging. 1989; 7:619–627. [PubMed: 2630844]
48. Wolf GL, Halavaara JT. Basic principles of MR contrast agents. Magn. Reson. Imaging Clin. N. Am. 1996; 4:1–10. [PubMed: 8673708]
49. Frank H, Weissleder R, Brady TJ. Enhancement of MR angiography with iron oxide: preliminary studies in whole-blood phantom and in animals. Am. J. Roentgenol. 1994; 162:209–213. [PubMed: 8273667]
50. Taupitz M, Schnorr J, Wagner S, et al. Coronary MR Angiography: Experimental Results with a Monomer-stabilized Blood Pool Contrast Medium. Radiology. 2002; 222:120–126. [PubMed: 11756715]
51. Sherry AD, Woods M. Chemical Exchange Saturation Transfer Contrast Agents for Magnetic Resonance Imaging. Annu. Rev. Biomed. Eng. 2008; 10:391–411. [PubMed: 18647117]
52. Van Zijl PCM, Yadav NN. Chemical exchange saturation transfer (CEST): What is in a name and what isn't? Magn. Reson. Med. 2011; 65:927–948. [PubMed: 21337419]
53. Sagiyama K, Mashimo T, Togao O, et al. In vivo chemical exchange saturation transfer imaging allows early detection of a therapeutic response in glioblastoma. Proc. Natl. Acad. Sci. 2014:201323855.
54. Ren J, Trokowski R, Zhang S, Malloy CR, Sherry AD. Imaging the Tissue Distribution of Glucose in Livers Using A PARACEST Sensor. Magn. Reson. Med. Off. J. Soc. Magn. Reson. Med. Soc. Magn. Reson. Med. 2008; 60:1047–1055.
55. Caravan P, Farrar CT, Frullano L, Uppal R. Influence of molecular parameters and increasing magnetic field strength on relaxivity of gadolinium- and manganese-based T1 contrast agents. Contrast Media Mol. Imaging. 2009; 4:89–100. [PubMed: 19177472]
56. Aime S, Botta M, Geninatti Crich S, Giovenzana G, Pagliarin R, Sisti M, Terreno E. NMR relaxometric studies of Gd(III) complexes with heptadentate macrocyclic ligands. Magn. Reson. Chem. 1998; 36:S200–S208.
57. Yerly F, Dunand FA, Tóth É, Figucirinha A, Kovács Z, Sherry AD, Geraldes CFGC, Merbach AE. Spectroscopic study of the hydration equilibria and water exchange dynamics of lanthanide(III) complexes of 1,7-bis(carboxymethyl)-1,4,7,10- tetraazacyclododecane (DO2A). Eur. J. Inorg. Chem. 2000:1001–1006.
58. Sherry AD, Wu Y. The importance of water exchange rates in the design of responsive agents for MRI. Curr. Opin. Chem. Biol. 2013; 17:167–174. [PubMed: 23333571]

59. Powell DH, Ni Dhubhghaill OM, Pubanz D, Helm L, Lebedev YS, Schlaepfer W, Merbach AE. Structural and dynamic parameters obtained from 17O NMR, EPR, and NMRD studies of monomeric and dimeric Gd3+ complexes of interest in magnetic resonance imaging: An integrated and theoretically self-consistent approach. J. Am. Chem. Soc. 1996; 118:9333–9346.
60. Siriwardena-Mahanama BN, Allen MJ. Strategies for optimizing water-exchange rates of lanthanide-based contrast agents for magnetic resonance imaging. Molecules. 2013; 18:9352–9381. [PubMed: 23921796]
61. Ruloff R, Tóth É, Scopelliti R, Tripier R, Handel H, Merbach AE. Accelerating water exchange for GDIII chelates by steric compression around the water binding site. Chem. Commun. 2002:2630–2631.
62. Jászberényi Z, Sour A, Tóth É, Benmelouka M, Merbach AE. Fine-tuning water exchange on GdIII poly(amino carboxylates) by modulation of steric crowding. Dalton Trans. 2005:2713–2719. [PubMed: 16075110]
63. Balogh E, Tripier R, Fousková P, Reviriego F, Handel H, Tóth E. Monopropionate analogues of DOTA4- and DTPA5-: Kinetics of formation and dissociation of their lanthanide(iii) complexes. Dalton Trans. 2007:3572–3581. [PubMed: 17680048]
64. Ferreira MF, Martins AF, Martins JA, Ferreira PM, Tóth E, Geraldes CFGC. Gd(DO3A-N-α-aminopropionate): A versatile and easily available synthon with optimized water exchange for the synthesis of high relaxivity, targeted MRI contrast agents. Chem. Commun. 2009:6475–6477.
65. André JP, Maecke HR, Tóth É, Merbach AA. Synthesis and physicochemical characterization of a novel precursor for covalently bound macromolecular MRI contrast agents. J. Biol. Inorg. Chem. 1999; 4:341–347. [PubMed: 10439079]
66. Zhang S, Kovacs Z, Burgess S, Aime S, Terreno E, Sherry AD. {DOTA-bis(amide)}lanthanide complexes: NMR evidence for differences in water-molecule exchange rates for coordination isomers. Chem. - Eur. J. 2001; 7:288–296. [PubMed: 11205022]
67. Aime S, Barge A, Bruce JI, Botta M, Howard JAK, Moloney JM, Parker D, De Sousa AS, Woods M. NMR, relaxometric, and structural studies of the hydration and exchange dynamics of cationic lanthanide complexes of macrocyclic tetraamide ligands. J. Am. Chem. Soc. 1999; 121:5762–5771.
68. Dunand FA, Borel A, Merbach AE. How does internal motion influence the relaxation of the water protons in LnIIIDOTA-like complexes? J. Am. Chem. Soc. 2002; 124:710–716. [PubMed: 11804502]
69. Caravan P. Protein-targeted gadolinium-based magnetic resonance imaging (MRI) contrast agents: Design and mechanism of action. Acc. Chem. Res. 2009; 42:851–862. [PubMed: 19222207]
70. Avedano S, Botta M, Haigh JS, L. Longo D, Woods M. Coupling fast water exchange to slow molecular tumbling in Gd3+ chelates: Why faster is not always better. Inorg. Chem. 2013; 52:8436–8450. [PubMed: 23841587]
71. Huang C-H, Tsourkas A. Gd-based macromolecules and nanoparticles as magnetic resonance contrast agents for molecular imaging. Curr. Top. Med. Chem. 2013; 13:411–421. [PubMed: 23432004]
72. Nicolle GM, Tóth É, Schmitt-Willich H, Radüchel B, Merbach AE. The impact of rigidity and water exchange on the relaxivity of a dendritic MRI contrast agent. Chem. - Eur. J. 2002; 8:1040–1048. [PubMed: 11891890]
73. Boros E, Polasek M, Zhang Z, Caravan P. Gd(DOTAla): A single amino acid Gd-complex as a modular tool for high relaxivity MR contrast agent development. J. Am. Chem. Soc. 2012; 134:19858–19868. [PubMed: 23157602]
74. Pierre, VC.; Allen, MJ.; Caravan, P. Contrast agents for MRI: 30+ years and where are we going? Topical issue on metal-based MRI contrast agents. In: Pierre, Valérie C., editor. J. Biol. Inorg. Chem. Vol. 19. 2014. p. 127-131.Guest editor
75. Aime S, Caravan P. Biodistribution of gadolinium-based contrast agents, including gadolinium deposition. J. Magn. Reson. Imaging. 2009; 30:1259–1267. [PubMed: 19938038]
76. Geraldes CFGC, Laurent S. Classification and basic properties of contrast agents for magnetic resonance imaging. Contrast Media Mol. Imaging. 2009; 4:1–23. [PubMed: 19156706]

77. Reimer P, Schneider G, Schima W. Hepatobiliary contrast agents for contrast-enhanced MRI of the liver: Properties, clinical development and applications. Eur. Radiol. 2004; 14:559–578. [PubMed: 14986050]

78. Giesel FL, Mehndiratta A, Essig M. High-relaxivity contrast-enhanced magnetic resonance neuroimaging: A review. Eur. Radiol. 2010; 20:2461–2474. [PubMed: 20567832]

79. Sena BF, Stern JP, Pandharipande PV, Klemm B, Bulman J, Pedrosa I, Rofsky NM. Screening Patients to Assess Renal Function Before Administering Gadolinium Chelates: Assessment of the Choyke Questionnaire. Am. J. Roentgenol. 2010; 195:424–428. [PubMed: 20651199]

80. Martin DR, Krishnamoorthy SK, Kalb B, et al. Decreased Incidence of NSF in Patients on Dialysis After Changing Gadolinium Contrast-Enhanced MRI Protocols. J. Magn. Reson. Imaging. 2010; 31:440–446. [PubMed: 20099361]

81. Abujudeh HH, Rolls H, Kaewlai R, Agarwal S, Gebreananya ZA, Saini S, Schaefer PW, Kay J. Retrospective assessment of prevalence of nephrogenic systemic fibrosis (NSF) after implementation of a new guideline for the use of gadobenate dimeglumine as a sole contrast agent for magnetic resonance examination in renally impaired patients. J. Magn. Reson. Imaging. 2009; 30:1335–1340. [PubMed: 19937927]

82. Moats RA, Fraser SE, Meade TJ. A “smart” magnetic resonance imaging agent that reports on specific enzymatic activity. Angew. Chem. - Int. Ed. Engl. 1997; 36:726–728.

83. Que EL, Chang CJ. Responsive magnetic resonance imaging contrast agents as chemical sensors for metals in biology and medicine. Chem Soc Rev. 2010; 39:51–60. [PubMed: 20023836]

84. Bonnet CS, Tóth E. MRI probes for sensing biologically relevant metal ions. Future Med Chem. 2010; 2:367–384. [PubMed: 21426172]

85. De Leon-Rodriguez L, Lubag AJM Jr, Dean Sherry A. Imaging free zinc levels in vivo - What can be learned? Inorg Chim Acta. 2012; 393:12–23.

86. Tu C, Louie AY. Strategies for the development of gadolinium-based “q”-activatable MRI contrast agents. NMR Biomed. 2013; 26:781–787. [PubMed: 23015370]

87. Brennan M-L, Penn MS, Van Lente F, et al. Prognostic Value of Myeloperoxidase in Patients with Chest Pain. N. Engl. J. Med. 2003; 349:1595–1604. [PubMed: 14573731]

88. Chen JW, Pham W, Weissleder R, Bogdanov A Jr. Human myeloperoxidase: A potential target for molecular MR imaging in atherosclerosis. Magn. Reson. Med. 2004; 52:1021–1028. [PubMed: 15508166]

89. Querol M, Chen JW, Weissleder R, Bogdanov A Jr. DTPA-bisamide-based MR sensor agents for peroxidase imaging. Org. Lett. 2005; 7:1719–1722. [PubMed: 15844889]

90. Nahrendorf M, Sosnovik D, Chen JW, Panizzi P, Figueiredo J-L, Aikawa E, Libby P, Swirski FK, Weissleder R. Activatable magnetic resonance imaging agent reports myeloperoxidase activity in healing infarcts and noninvasively detects the antiinflammatory effects of atorvastatin on ischemia-reperfusion injury. Circulation. 2008; 117:1153–1160. [PubMed: 18268141]

91. Overoye-Chan K, Koerner S, Looby RJ, Kolodziej AF, Zech SG, Deng Q, Chasse JM, McMurry TJ, Caravan P. EP-2104R: A fibrin-specific gadolinium-based MRI contrast agent for detection of thrombus. J. Am. Chem. Soc. 2008; 130:6025–6039. [PubMed: 18393503]

92. Caravan P, Das B, Dumas S, et al. Collagen-targeted MRI contrast agent for molecular imaging of fibrosis. Angew. Chem. - Int. Ed. 2007; 46:8171–8173.

93. Esqueda AC, López JA, Andreu-de-Riquer G, Alvarado-Monzón JC, Ratnakar J, Lubag AJM, Sherry AD, De León-Rodríguez LM. A new gadolinium-based MRI zinc sensor. J. Am. Chem. Soc. 2009; 131:11387–11391. [PubMed: 19630391]

94. Lubag AJM, De Leon-Rodriguez LM, Burgess SC, Sherry AD. Noninvasive MRI of β-cell function using a Zn 2+-responsive contrast agent. Proc. Natl. Acad. Sci. U. S. A. 2011; 108:18400–18405. [PubMed: 22025712]

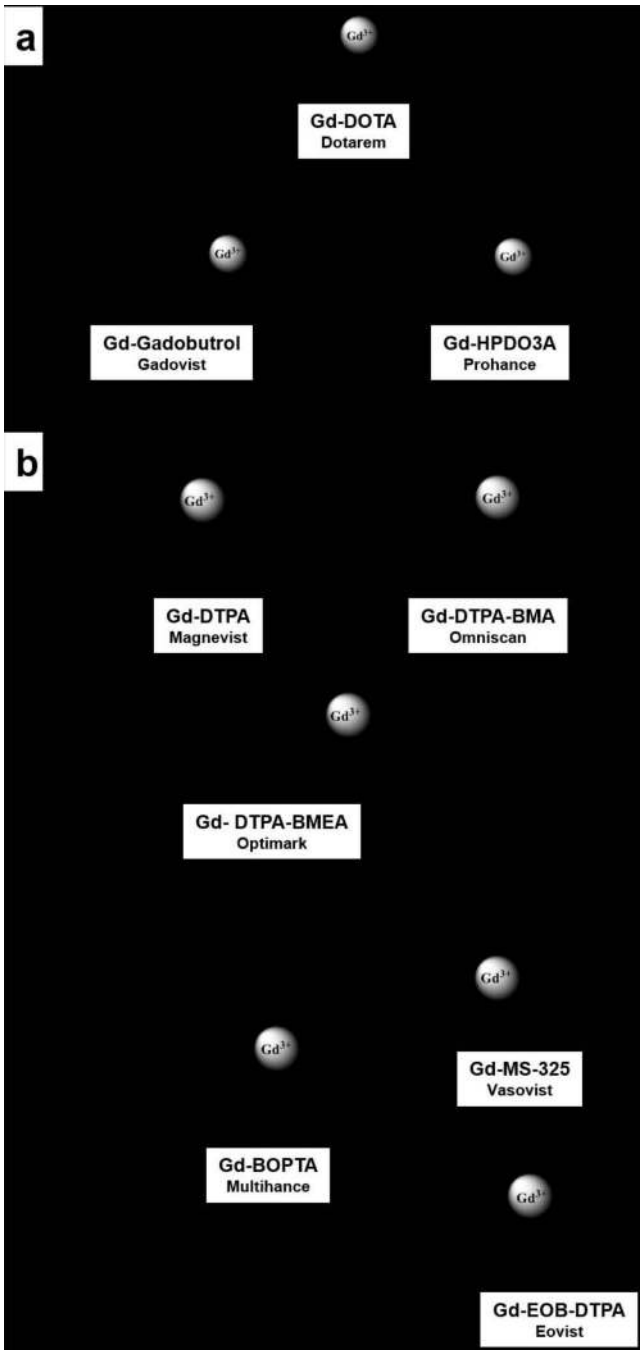


**Figure 1.**

Schematic representation of commercially available and clinical $Gd^{3+}$-based contrast agents: a) polyaza macrocycles, b) linear polyaminocarboxylates.

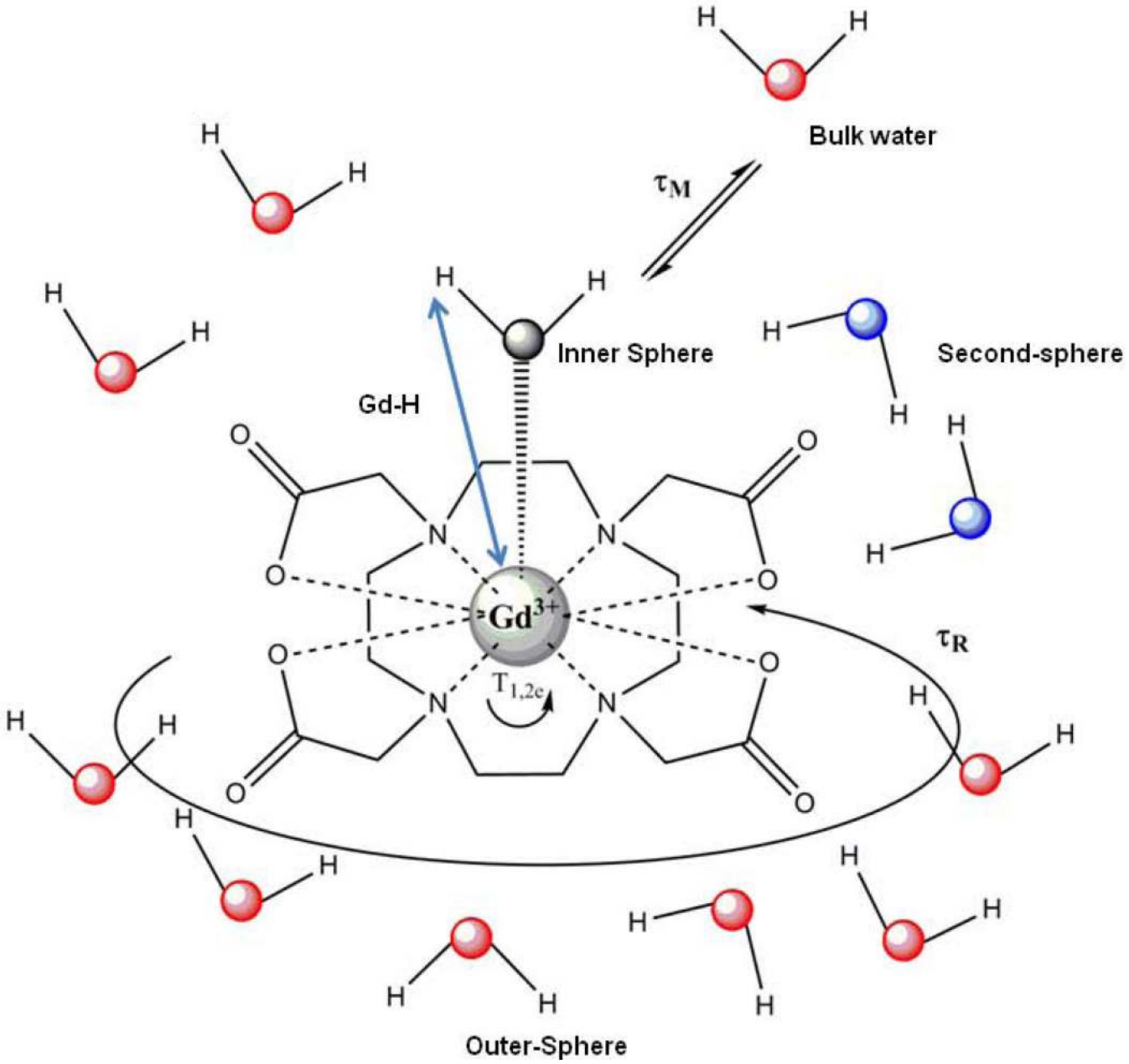


**Figure 2.**

Schematic representation of a $Gd^{3+}$-complex (GdDOTA) with one coordinated water molecule (*inner-sphere* water, its oxygen is colored black) in solution (*bulk water*, oxygens are red). *Second-sphere* water molecules (water oxygens are blue) are close to the carboxylate groups with their hydrogens oriented towards the carboxylate oxygens. The parameters that govern the relaxivity are also represented: Gd-H distance, the mean lifetime ($\tau_m$) of the water molecule(s) in the inner sphere, the rotational correlation time ($\tau_R$) and the electronic spin relaxation times ($T_{1e}$ and $T_{2e}$). For clinical agents, approximately 60% of the relaxivity originates from inner sphere relaxation and 40% from outer sphere effects.

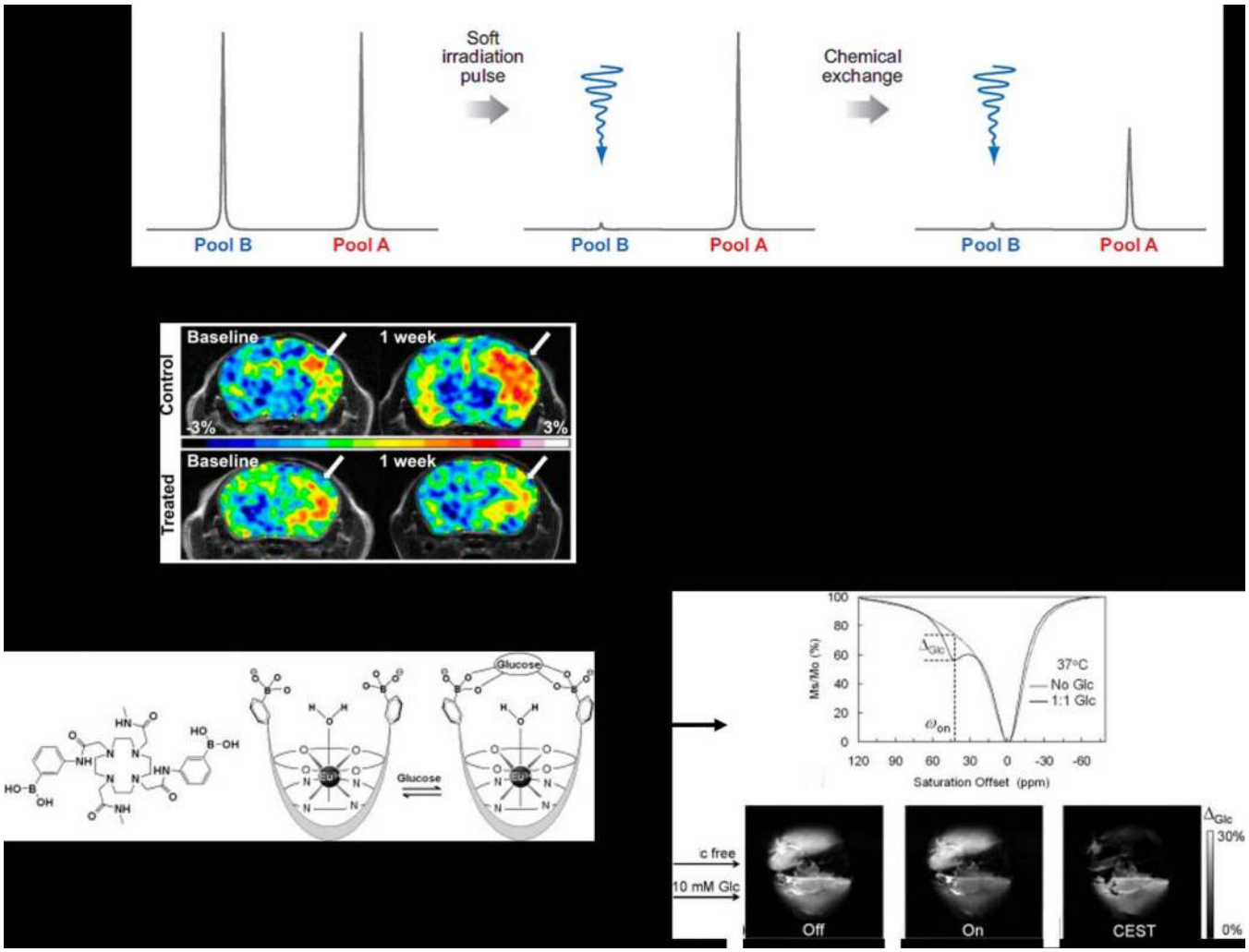


**Figure 3.**

**A)** All illustration of two chemical types of protons in exchange with one another. Selective saturation of pool B for a period of a few seconds results in a decrease in intensity of pool A (51). **B)** An example of endogenous CEST in an orthotopic glioblastoma multiform (GBM) tumor in a mouse. Presaturation of all exchangeable amide protons at 3.5 ppm downfield of water results in a larger CEST signal in the tumor compared to the surrounding healthy brain. The bottom images illustrate that the CEST signal decreases after one round of temozolomide (TMZ) chemotherapy, the standard drug used in GBM patients. **C)** An example of an exogenous CEST agent. Here, a $Eu^{3+}$ macrocyclic ligand complex was designed to bind glucose. This glucose sensor shows no CEST signal in the absence of glucose but a strong CEST signal after addition of glucose. This has been used to image the extracellular distribution of glucose in a perfused liver model. Molecular sensors such as could ultimately prove useful in differentiating between livers producing normal amounts of glucose versus livers over-producing glucose such as in patients with type II diabetes. Reproduced from (46,54).

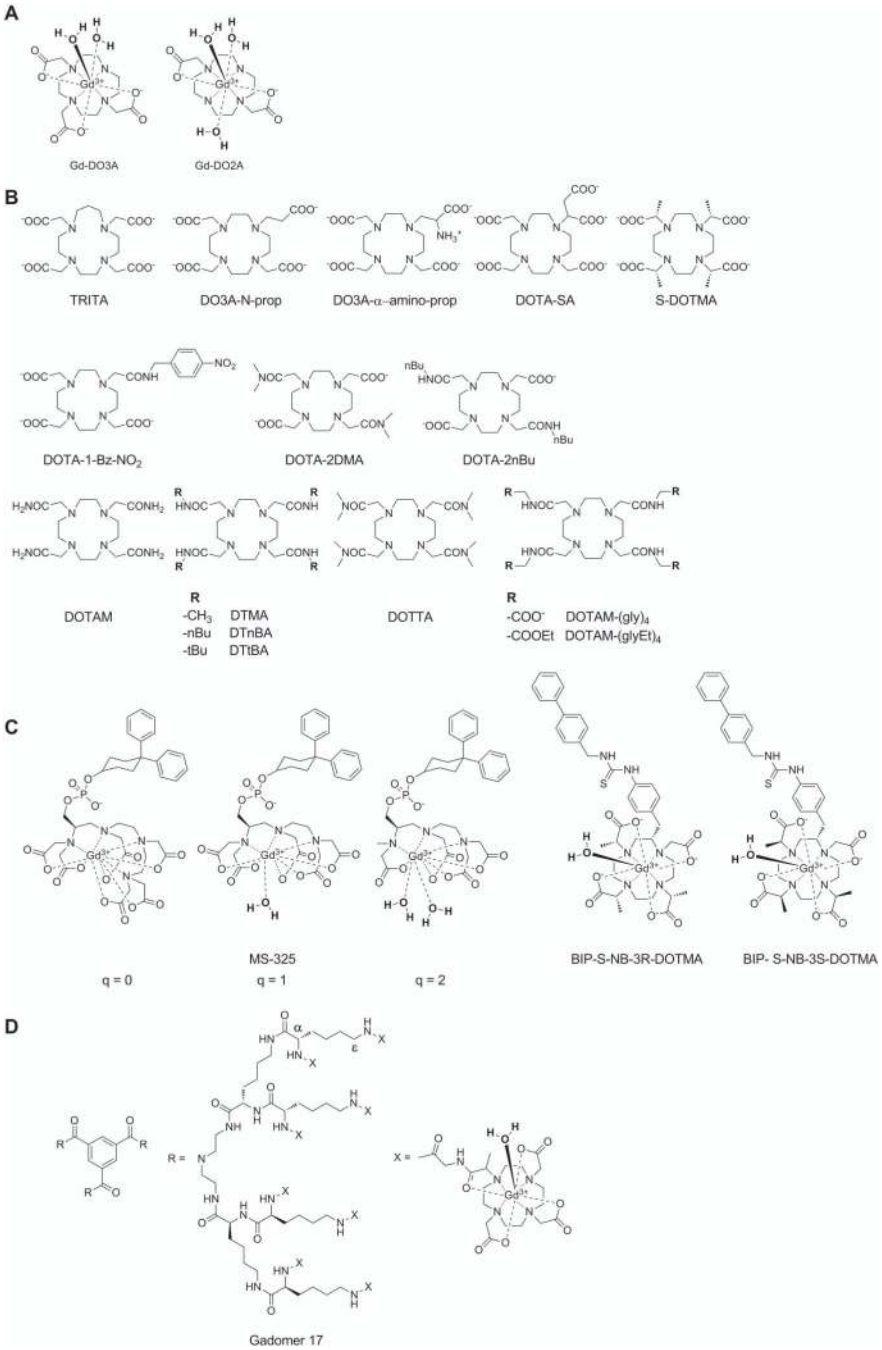


**Figure 4.**

Structures of the some $Gd^{3+}$ complexes and ligands discussed in this paper.

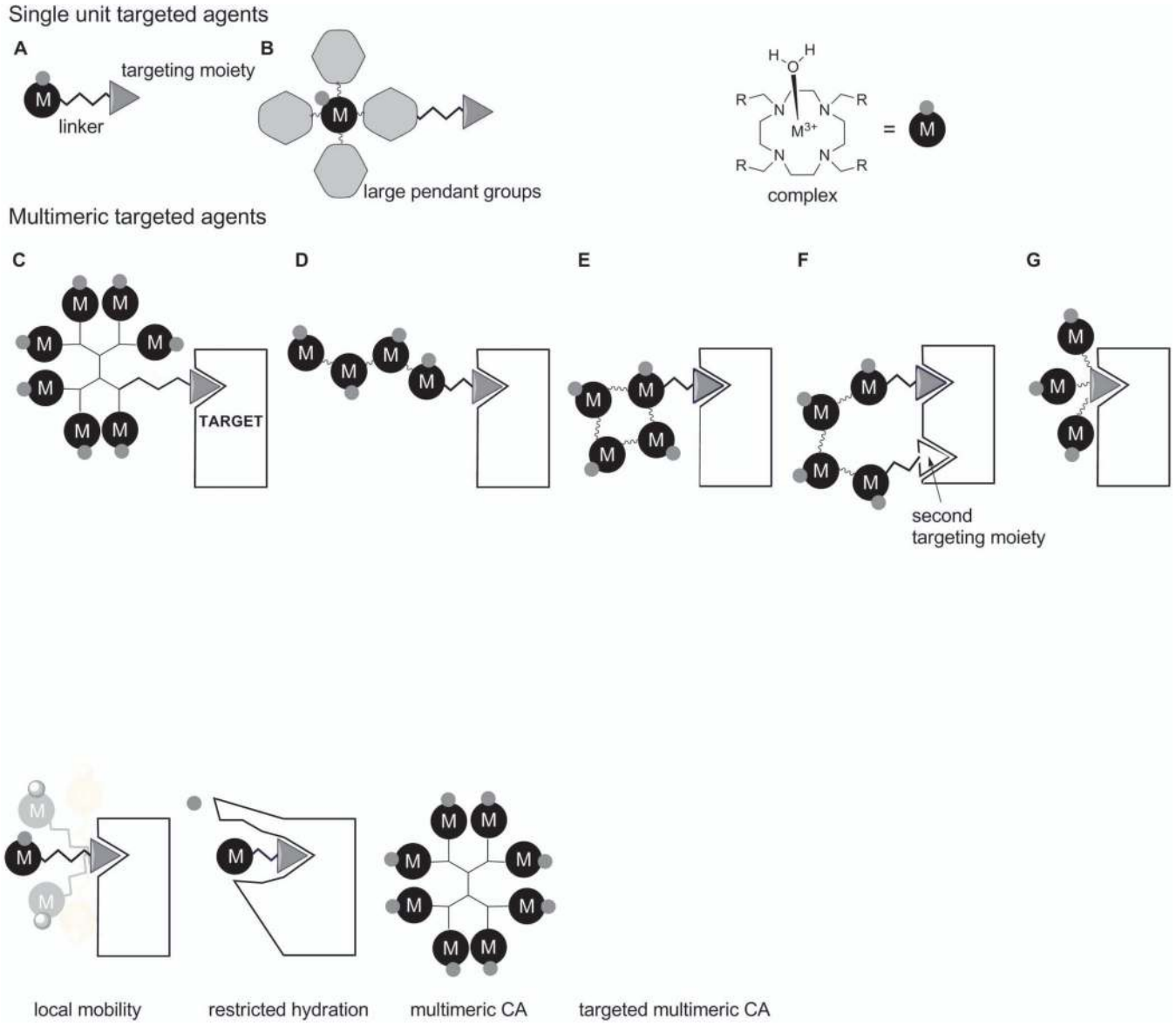


**Figure 5.**

Designs of monomeric and multimeric contrast agents. **A)** Simple targeting unit, where the $Gd^{3+}$ complex is attached to the targeting moiety through a linker. **B)** The metal ion is placed at the barycenter of a molecule designed to limit molecular rotation. One can also increase sensitivity by increasing the number of $Gd^{3+}$ ions bound at the target site by use of a dendrimer **C)** or a straight-chain polymer **D)**. The relaxivity gains due to restriction rotation can be quite small in **C)** and **D)** so other approaches to restrict motion by having multiple points of attachment near the target are illustrated in **E)**, **F)** and **G)**. In these illustrations, the black circled 'M's denote ML complexes and the smaller, associated gray circles represent a single water molecule on each chelate.

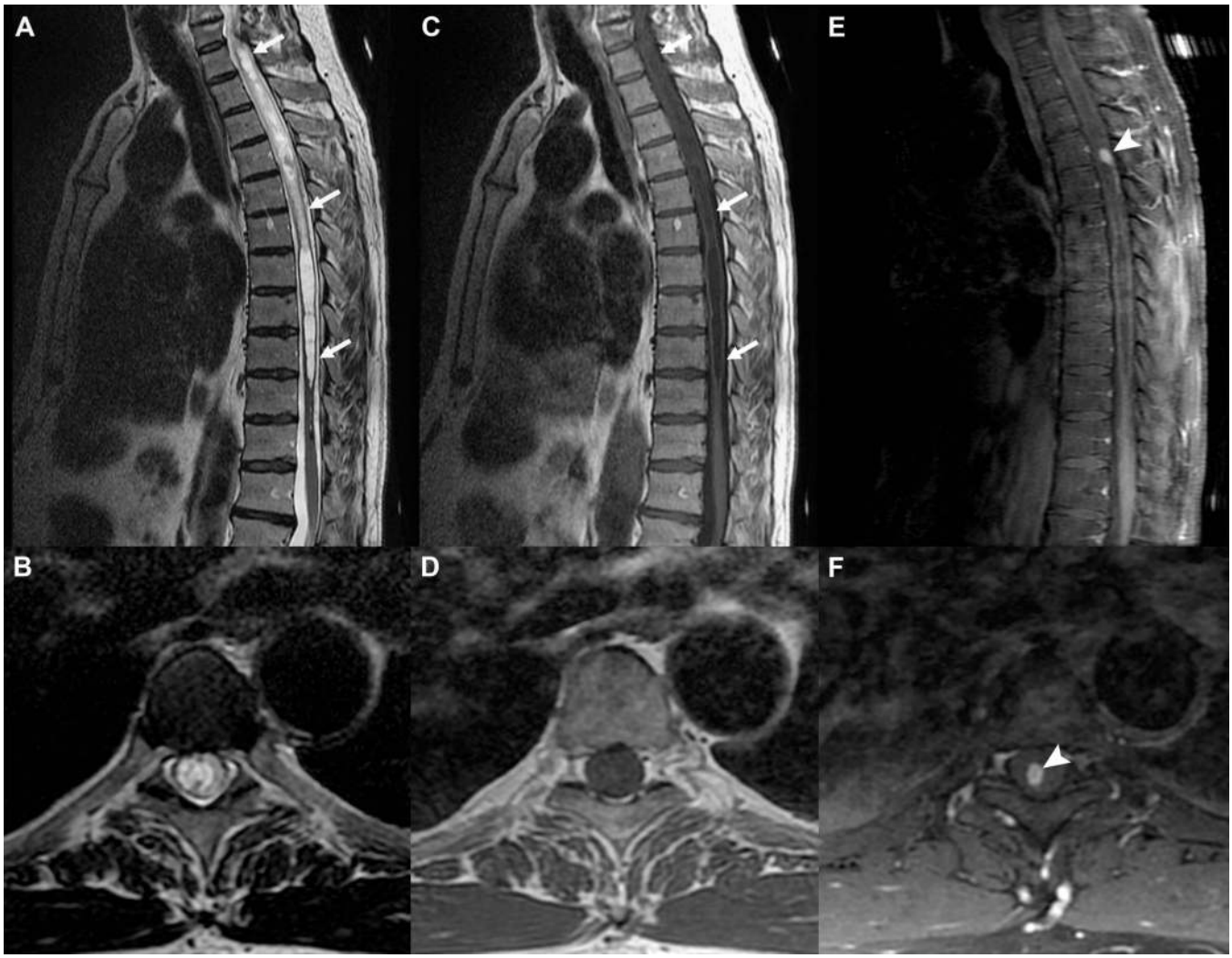


**Figure 6.**

Gd-based CA for detection of CNS neoplasm. Sagittal and axial T2-weighed (A and B) and T1-weighed (C and D) FSE acquisitions with an extensive thoracic syrinx (white arrows) in a patient with progressive neurological deficits. The etiology remains obscure. Post contrast T1-weighed FSE acquisitions in the sagittal (E) and axial (F) planes demonstrate a small avidly enhancing nodule (arrowheads), which was resected and proven to be a hemangioblastoma (benign hypervascular neoplasm). Without the added information from the CA, the syrinx would be considered idiopathic and no treatment options would be available.

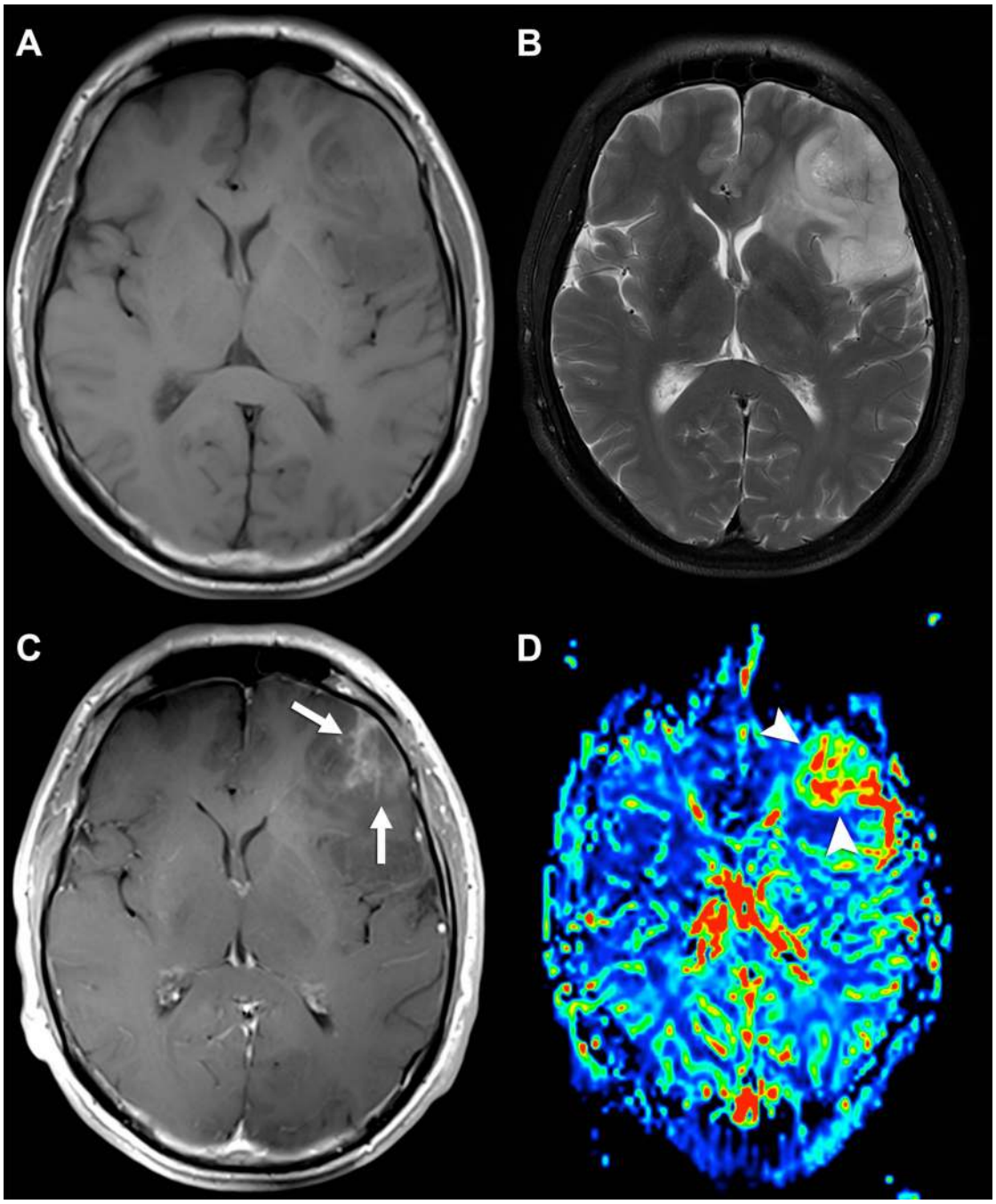


**Figure 7.**

Value of Gd-based CA for glioma characterization. Axial T1-weighted (**A**) and T2-weighted (**B**) FSE acquisitions demonstrating a large left infiltrative mass consistent with a glial neoplasm, but of uncertain aggressiveness. Post contrast axial T1-weighed FSE acquisition (**C**) demonstrates a focal region of heterogeneous enhancement (white arrows), a finding usually seen in malignant gliomas. CMV map (D) from T2* bolus dynamic susceptibility contrast (DSC) acquisition demonstrates a focal area of markedly increased tumor

vascularity (arrowheads) matching the area of enhancement. This area was targeted for stereotatic biopsy, which confirmed the suspicion of an anaplastic glioma.

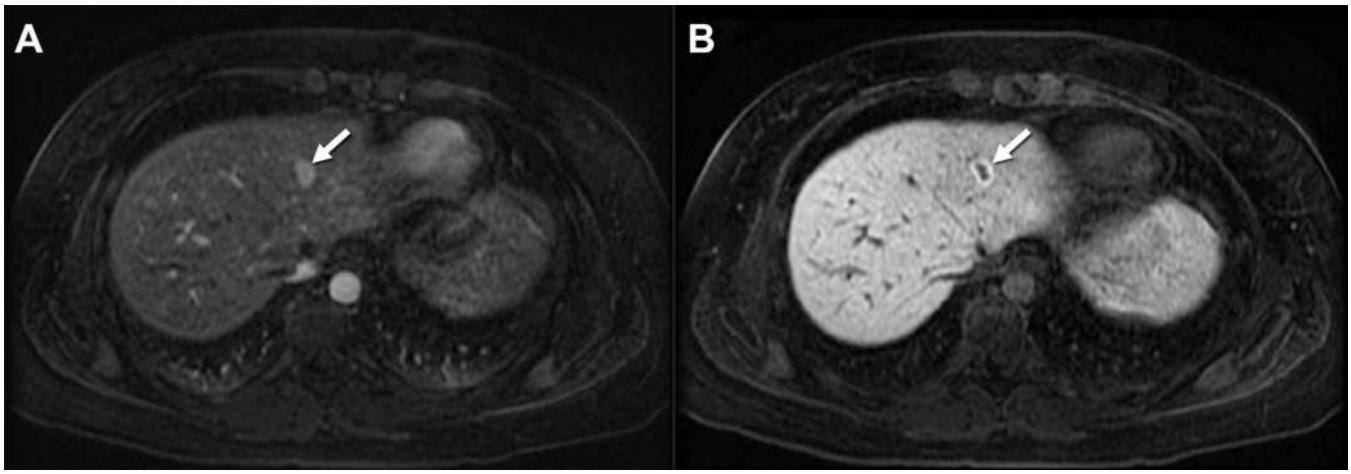


**Figure 8.**

Use of *Gd-EOB-DTPA* for characterization of Focal Nodular Hyperplasia. Fat suppressed 3D T1-weighted images obtained during the arterial phase (**A**) and at 20 minutes (**B**) after the intravenous administration of 0.025 mmol/kg gadoxetic acid. Note the high signal intensity of the focal mass in the left lobe of the liver (arrow) on the arterial phase with sustained enhancement of the lesion on the delayed phase, the latter including substantial diffuse background liver enhancement.

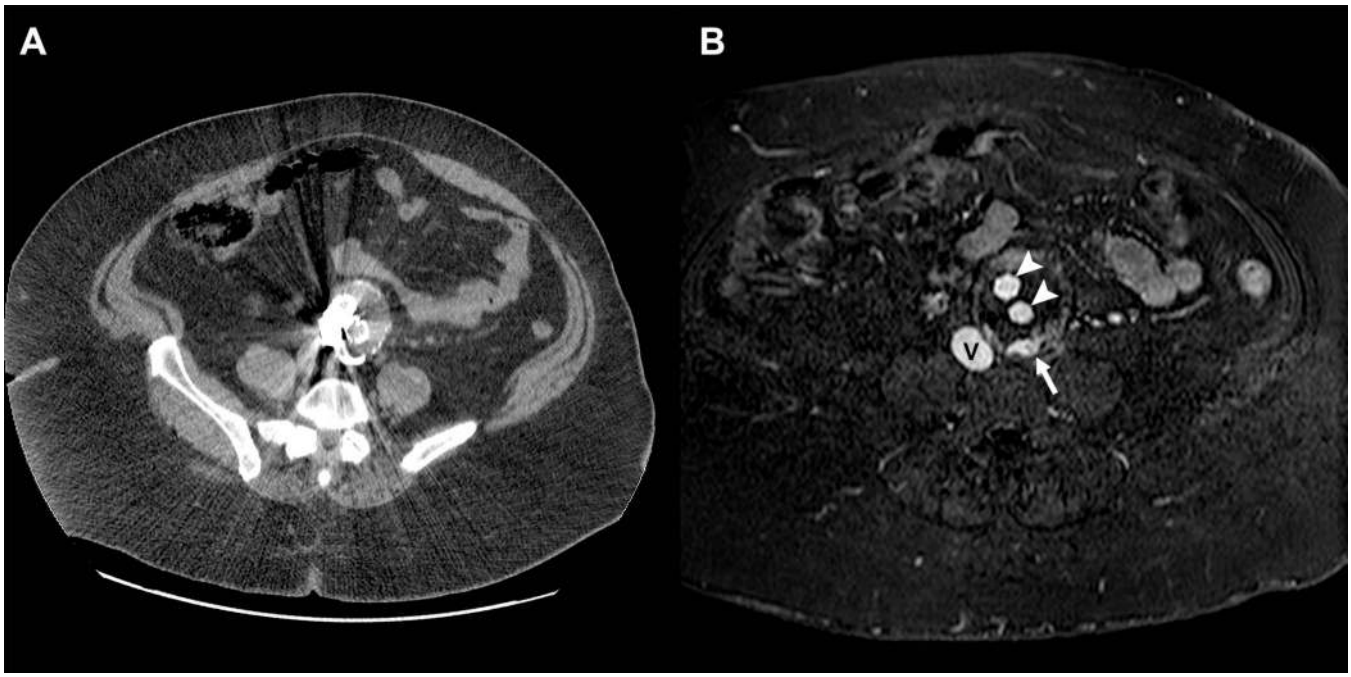


**Figure 9.**

Clinical application of the blood pool properties of gadofosveset trisodium during follow-up of a patient with an aortic aneurysm. Contrast enhanced computed tomographic scan (**A**) was of limited diagnostic value due to prominent streak artifacts from metal. GdMS-325 contrast-enhanced magnetic resonance angiography during a blood pool phase acquisition demonstrates excellent signal intensity on the inferior vena cava (**V**) as well as in the arterial prosthesis (arrowheads).. The white arrow demonstrates an endoleak, which was not detected on CT.

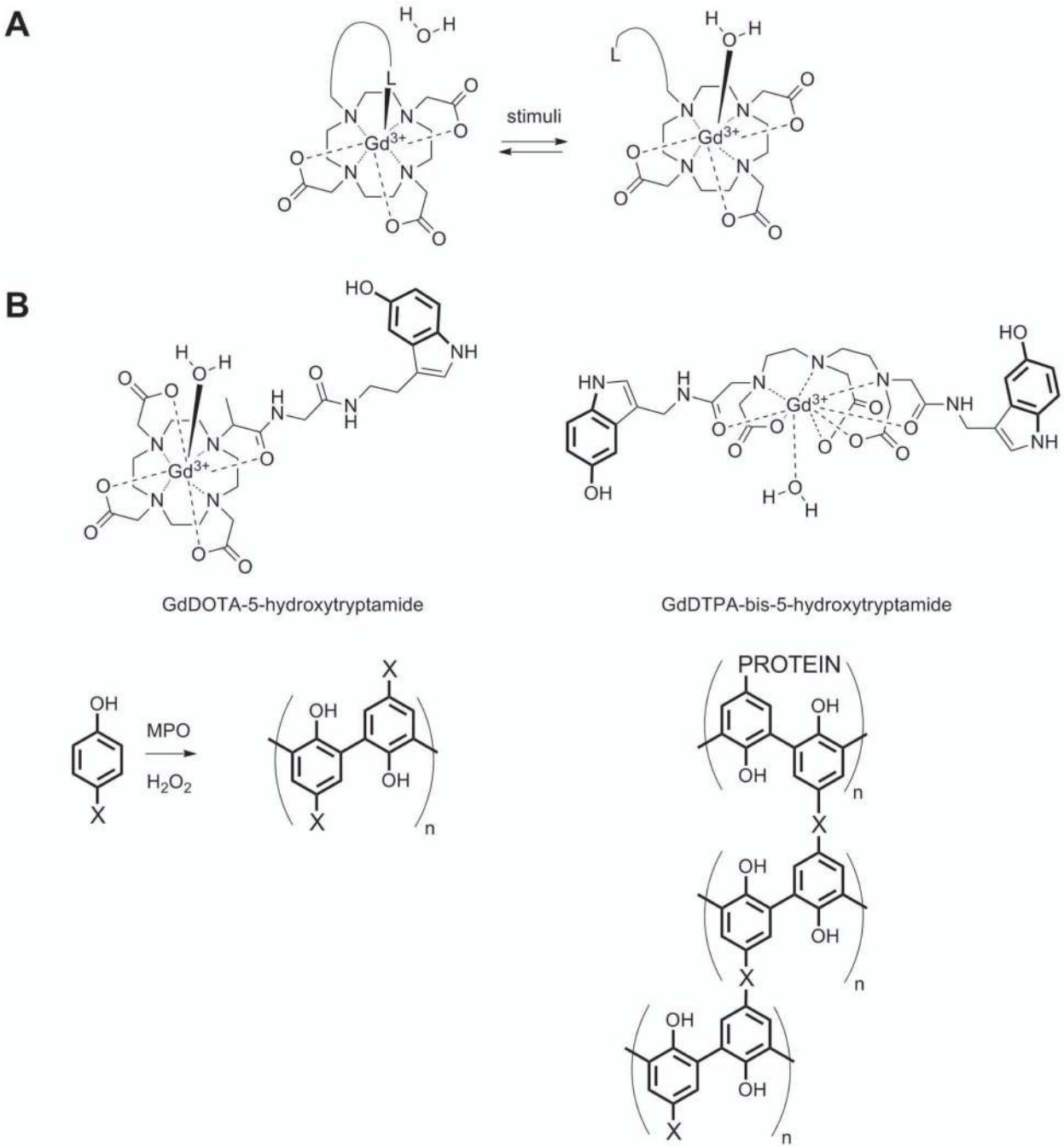


**Figure 10.**

**A)** A model *q*-responsive agent in which increases water access to the inner coordination sphere of the $Gd^{3+}$. The symbol "L" refers to a ligand that binds to the $Gd^{3+}$ prior to stimulation and moves away from the water binding site after stimulation. One example of this would be the β-D-galactose residue in E-Gad (86). **B)** Examples of myeloperoxidase-responsive contrast agents, where X corresponds to a $Gd^{3+}$ complex. One example with X = GdDTPA-bis-5-hydroxytryptamide provided prolonged enhancement in injured myocardium compared with a control.

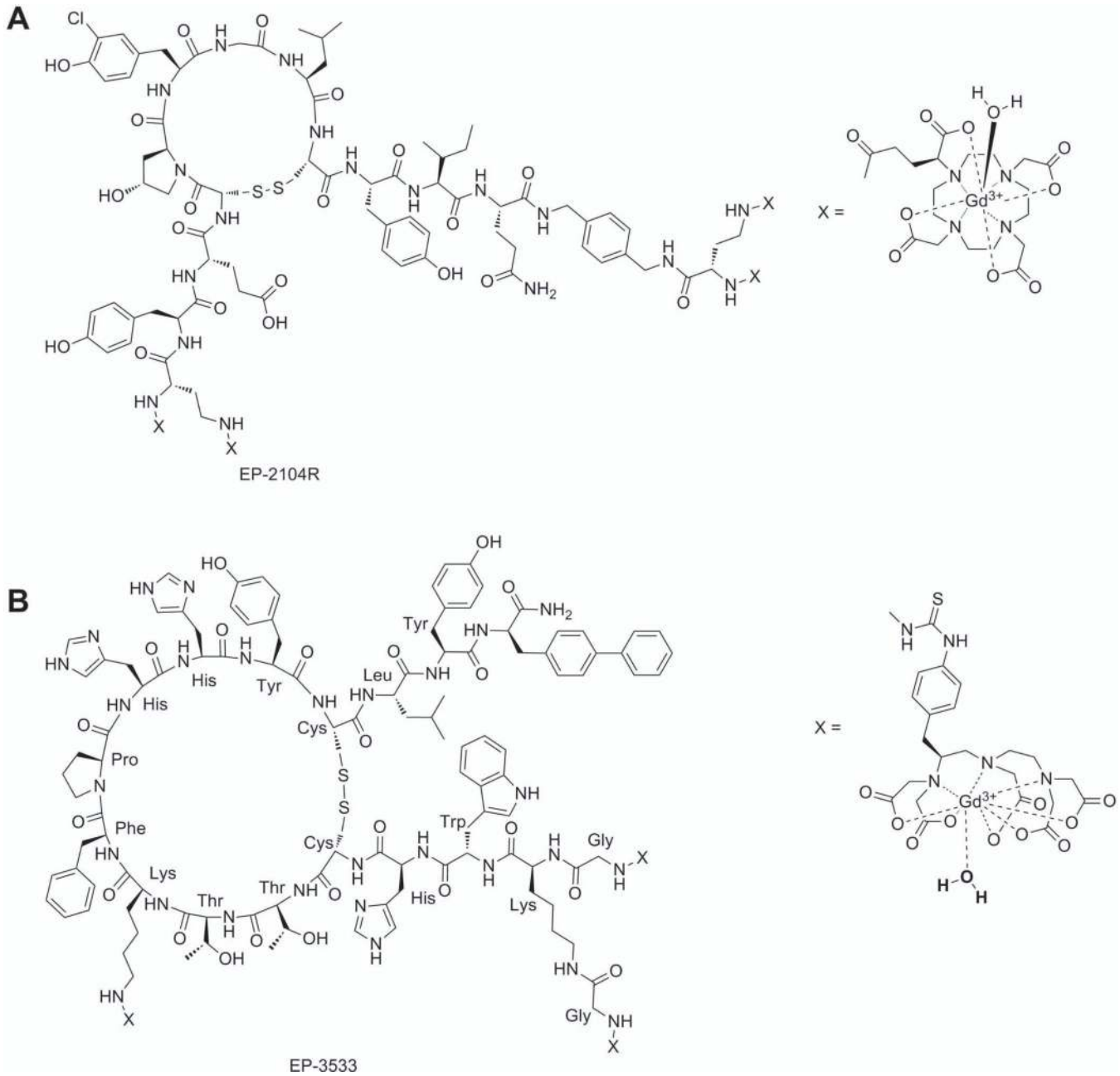


**Figure 11.**

**A**) Fibrin and **B)** collagen targeting MRI agents.

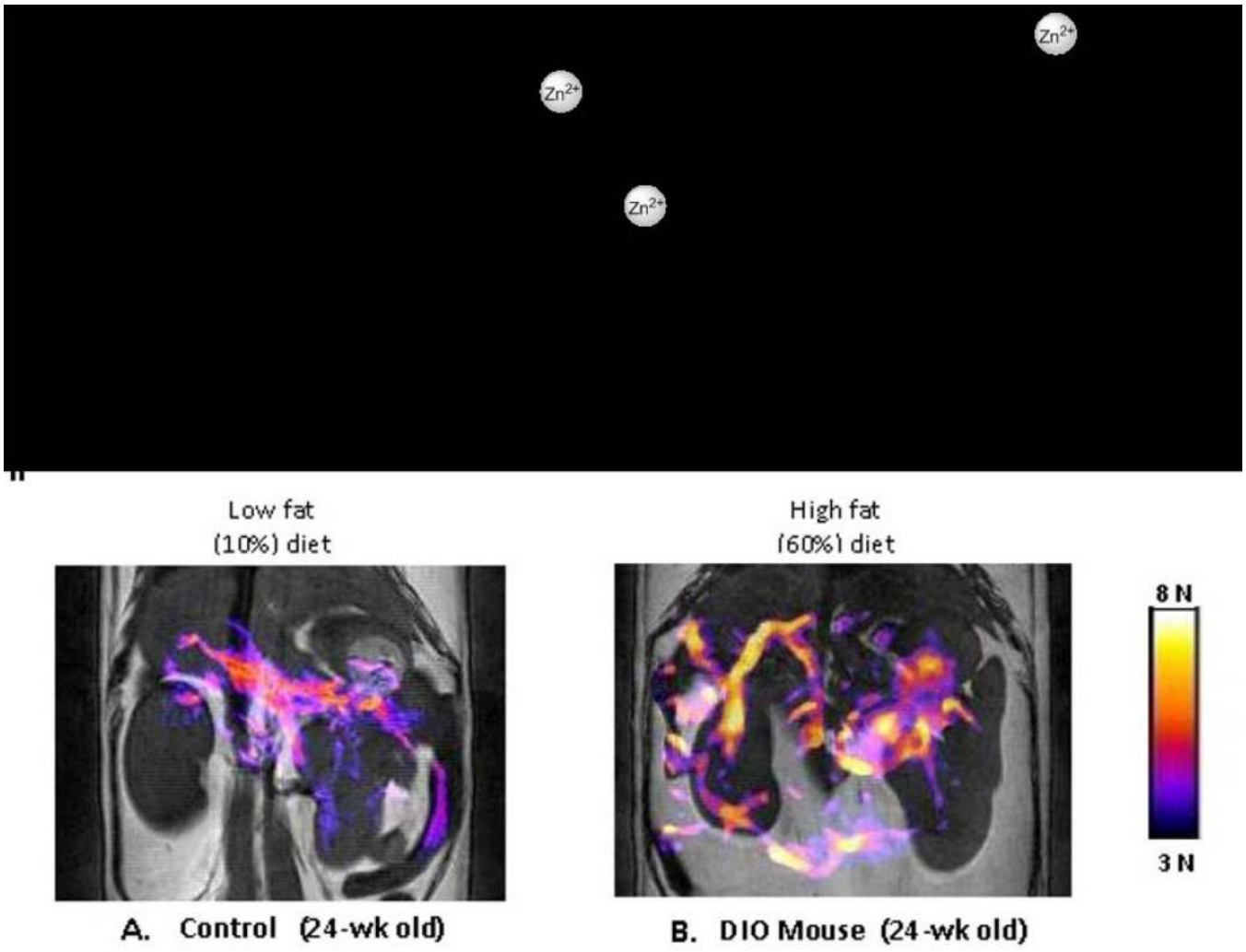


**Figure 12.**

**I)** A $Gd^{3+}$-based macrocyclic agent that acts as a MRI sensor of free $Zn^{2+}$ ions *in vivo*. **II**) Simulation of insulin secretion from pancreatic β-cells by glucose results in co-release of high levels of free $Zn^{2+}$ ions packaged with insulin in β-cell granules. The colored areas shown in these images reflect functional release of $Zn^{2+}$ and insulin in these mice. The mouse on the right was fed a high fat diet for 12 weeks to expand β-cell mass. The expanded colored areas in this image reflect a larger functional pancreas (increased β-cell function) in this animal. This process is known to occur in diet-induced obesity (DIO) mouse models (94). Functional agents such as this may one day allow imaging of β-cell function in humans during development of type II diabetes or as a biomarker to test new drugs designed to improve β-cell function.

**Table 1**

Thermodynamic stability constants (log $K_{st}$), proton relaxivities ($r_1$), bound water lifetimes ($\tau_m$), dissociation rate constants ($k_1$ and $k_{obs}$), and dissociation half-life at pH = 1 ($T_{1/2}$) for some $Gd^{3+}$-based CA.

| Chemical name Linear (L) or Macrocycle (M) | Generic Name | $r_1$ ($mM^{-1}s^{-1}$) [a] (7) | | | $\tau_m$ (ns) (8) | log $K_{st}$ (9) | $k_1$ ($M^{-1}.s^{-1}$ (10) | $k_{obs}$ ($s^{-1}$) (10,11) | $T_{1/2}$ (10–12) |
|---|---|---|---|---|---|---|---|---|---|
| | | 0.47T | 1.5T | 3T | | | | | |
| GdDTPA (L) | Gadopentetate dimeglumine | 3.4 (13) | 3.3 | 3.1 | 143 | 22.46 (14) | 0.58 | $1.2 \times 10^{-3}$ | 9.6 min |
| GdDOTA (M) | Gadoterate meglumine | 3.4 (13) | 2.9 | 2.8 | 122 | 25.30 (15) | - $2.0 \times 10^{-5}$ $8.4 \times 10^{-6}$ | $2.1 \times 10^{-5}$ $2.0 \times 10^{-6}$ (16) $8.4 \times 10^{-7}$ (10) | ~9 hr 96[a] 229 hr |
| GdDTPA-BMA (L) | Gadodiamide | 3.5 (17) | 3.3 | 3.2 | 967 | 16.85 (18) | 12.7 | $> 2 \times 10^{-2}$ | <34 s |
| GdHP-DO3A (M) | Gadoteridol | 3.1[b] (19) | 2.9 | 2.8 | 51 | 23.80 (20) | $6.4 \times 10^{-4}$ | $6.4 \times 10^{-5}$ | 3 hr |
| GdDO3-Abutrol (M) | Gadobutrol | 3.60[b] (21) | 3.3 | 3.2 | 57 | 21.80 (20) | $2.8 \times 10^{-5}$ | $2.8 \times 10^{-6}$ | 68 hr |
| GdDOTA- $(gly)_4$ (M) | Not available | 2.10 (22) | | | 7700[c] (23) | 14.54 (22) | $8.1 \times 10^{-6}$ | $1.6 \times 10^{-6}$ | 125 hr |
| GdDTPA-BMEA (L) | Gadoversetamide | 4.2[b] | 3.8 | 3.6 | 71 | 16.84 (15) | 8.6 (24) | - | - |
| GdEOB-DTPA (L) | Gadoxetate disodium | 5.3 | 4.7 | 4.3 | 82 | 23.5 | 0.16 (25) | - | - |
| GdMS-325 (L) | Gadofosveset trisodium | 5.8 28[d] | 5.3 19[d] | 5.2 9[d] | 69 | 22.1 (26) | [e] (26) | - | - |
| GdBOPTA (L) | Gadobenate disodium | 4.2 | 4.0 | 4.0 | 140 | 22.6 | 0.41 (25,27) | - | - |

Relaxivities in water at

[a] 37°C and

[b] 40°C.

[c] Measured at 22°C.

[d] Measured in plasma.

[e] Reported to be at least 10–100 times better than GdDTPA.